Conformation and Dynamics of DNA and Protein–DNA Complexes by ^{31}P NMR

David G. Gorenstein

Department of Chemistry, Purdue University, West Lafayette, Indiana 47907

Received December 3, 1993 (Revised Manuscript Received April 8, 1994)

Contents

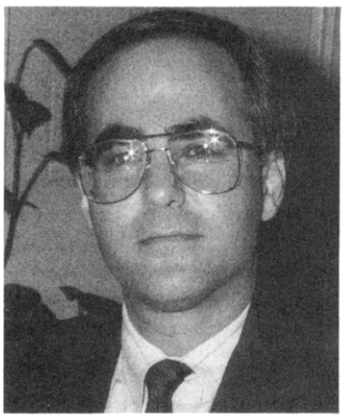

David Gorenstein is Professor of Chemistry at Purdue University and Director of the Purdue Biochemical Magnetic Resonance Laboratory. He was born in Chicago and educated in the Boston area, with a 1966 B.S. degree from M.I.T. and a Ph.D. with Frank Westheimer at Harvard in 1969. He then directly joined the University of Illinois at Chicago where he stayed except for a one-year Senior Fulbright Fellowship at Oxford University in England. In 1985 he moved to Purdue University, West Lafayette, IN, and shortly afterward completed a Guggenheim Fellowship at University of California, San Francisco. His research interests include NMR spectroscopy of biological macromolecules, enzymology, and theoretical organic chemistry, particularly of phosphorus compounds. More recently he has become involved in protein and drug design.

1. Introduction

^{31}P NMR has developed as a powerful probe of the structure and dynamics of nucleic acids and nucleic acid complexes in solution. Until recently ^{31}P NMR studies of nucleic acids were restricted to partial identification of signals for polymeric nucleic acids and oligodeoxyribonucleotide sequences less than six base pairs in length.[1] However, synthetic schemes have now been developed where defined deoxy- (and more recently ribo- and backbone modified) oligonucleotides can be routinely produced in multimilligram quantities.[2,3] The concomitant development of sequence-specific 2D $^1H/^1H$ and 2D and 3D $^1H/^{31}P$ NMR assignment methodologies[4–14] has made the assignment of the ^{31}P NMR spectrum of modest side oligonucleotides (8–14 base pairs) possible.

One of the main reasons for assigning ^{31}P resonances of oligonucleotides is to obtain information on the conformation of the phosphodiester backbone (Figure 1).[15–19] The internucleotide linkage is defined by six torsional angles from one phosphate atom to the next along the DNA backbone. Theoretical studies have shown that the conformation of two of the six torsional angles (α, O3′–P–O5′–C5′, and ζ, C3′–O3′–P–O5′) appear to be most important in determining ^{31}P chemical shifts.[15,18,20] Molecular dynamics calculations,[21] X-ray diffraction,[22] and 2D NMR[23–25] spectroscopy have also shown that the phosphate ester conformation is the most variable part of nucleic acid structure.[26] As discussed in this review, ^{31}P chemical shifts and $^1H–^{31}P$ coupling constants can provide valuable information on the phosphodiester backbone conformation.

It is now widely appreciated that significant local conformational heterogeneity exists in the structures of nucleic acids.[27–30] While X-ray crystallography has provided much of our understanding of largely DNA

0009-2665/94/0794-1315$14.00/0

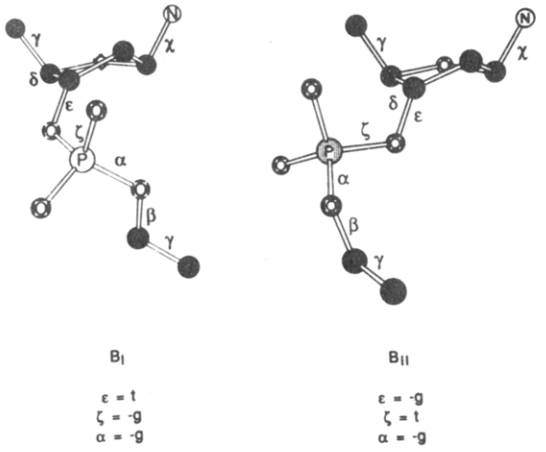

Figure 1. Stereoview of sugar phosphate backbone (A) in B_I conformational state (B) in B_{II} conformational state. Torsional angles α, β, ϵ, ζ: g^-, t, t, g^- (A); g^-, t, g^-, t (B). The B_I conformation represents the low-energy phosphate state normally observed in the crystal structures for many of the duplex phosphates and the B_{II} conformation represents the other major sugar phosphate state for B-DNA. Torsional angles are gauche(–) (g^- or –60°) and trans (180°). Crystal structures of duplex oligonucleotides show that these angles are only approximate and indeed the ζ angle is generally closer to –90° for what is defined as "g^-".

duplex structural variations, increasingly, high-resolution multidimensional NMR has provided detailed three-dimensional structural information on duplex, hairpin loops, and other oligonucleotide structures. Importantly NMR experiments have suggested that the nucleic acid conformation in solution[20,31–35] may not be identical to the static picture provided by X-ray diffraction in the crystal state.

Traditionally the phosphate ester moiety is often overlooked and viewed as a passive element of nucleic acid structure. Base pairing and other nucleic acid base oriented structural features have been assumed to control nucleic acid structure and conformation. More recently (and as discussed in this review) we have begun to appreciate the important role played by the phosphate ester in defining the structure and dynamics of nucleic acids as well as nucleic acid–drug or –protein complexes.

Thus, most attention on understanding the recognition specificity between DNA binding proteins and DNA sequences has centered on hydrogen bonding to the acceptor/donor groups on the Watson–Crick base pairs in the major groove (cf. ref 36). Even with the extensive X-ray and NMR studies on this problem, we still do not understand this "second genetic code" of protein–DNA recognition. Perhaps one reason for the inability to dissect the basis for this specificity is the emphasis on base-pair interactions alone. Localized, sequence-specific conformational variations in DNA are quite likely another important component of a protein's recognition of specific sites on the DNA.[36,37] Thus, although the *lac* repressor protein does not recognize an alternating AT sequence as part of the *lac* operator DNA sequence, the repressor protein binds to poly-[d(AT)] 1000 times more tightly than to random DNA.[29] Repressor protein is quite likely recognizing the alternating deoxyribose phosphate backbone geometry of the two strands,[38] rather than the chemical identity of the AT base pairs.

Remarkably, in every high-resolution X-ray crystal structure of a protein–DNA complex, the majority of the contacts are to the phosphates![39–44] Indeed, the crystal structure of the *trp* repressor demonstrated that every one of the nearly two dozen direct protein contacts were mediated through interactions with the phosphate backbone.[41] While some controversy exists as to the correctness of this complex,[45,46] more recent results confirm the specificity of this operator complex.[47] In another recent CAP–DNA complex it would appear that 22 out of the 28 contacts are also to the phosphates;[48] these include protein backbone amide H-bonds, side-chain H-bonds, and charged interactions. It is not known whether any of these ionic interactions provide a specific recognition mechanism for these repressors. As described in this review, the conformation and, in particular, the flexibility of the phosphates may be an important component of protein–DNA recognition.

Additional reviews of the earlier literature on ^{31}P NMR studies of duplex polynucleotides by Cohen[49] and on duplex oligonucleotides[50] and drug–DNA complexes[51] are recommended. Excellent discussions of solid-state DNA studies by Tsai[52] and phosphorus relaxation methods by Hart[53] and James[54] are also recommended.

2. *Phosphorus-31 Chemical Shifts*

1. Introduction and Basic Principles

The interaction of the electron cloud surrounding the phosphorus nucleus with an external applied magnetic field H_0 gives rise to a local magnetic field. This induced field shields the nucleus, with the shielding proportional to the field H_0 so that the effective field, H_{eff}, felt by the nucleus is given by

$$H_{eff} = H_0(1 - \sigma) \tag{1}$$

where σ is the shielding constant. Because the charge distribution in a phosphorus molecule will generally be far from spherically symmetrical, the ^{31}P chemical shift (or shielding constant) varies as a function of the orientation of the molecule relative to the external magnetic field.[55–59] This gives rise to a chemical-shift anisotropy that can be defined by three principal components σ_{11}, σ_{22}, and σ_{33} of the shielding tensor.[55] For molecules that are axially symmetrical, with σ_{11} along the principal axis of symmetry, $\sigma_{11} = \sigma_\parallel$ (parallel component), and $\sigma_{22} = \sigma_{33} = \sigma_\perp$ (perpendicular component). These anisotropic chemical shifts are observed in solid samples[56–60] and liquid crystals,[61] whereas for small molecules in solution, rapid tumbling averages the shift. The average, isotropic chemical shielding σ_{iso} (which would be comparable to the solution chemical shift) is given by the trace of the shielding tensor or

$$\sigma_{iso} = {}^1/_3(\sigma_{11} + \sigma_{22} + \sigma_{33}) \tag{2}$$

and the anisotropy $\Delta\sigma$ is given by

$$\Delta\sigma = \sigma_{11} - {}^1/_2(\sigma_{22} + \sigma_{33})$$

or, for axial symmetry,

$$\Delta\sigma = \sigma_\parallel - \sigma_\perp \tag{3}$$

2. Theoretical ^{31}P Chemical Shift Calculations and Empirical Observations

Several attempts have been made to develop a unified theoretical foundation for ^{31}P chemical shifts of phos-

phorus compounds.[62-67] In one theoretical approach, Letcher and Van Wazer,[62,63] using approximate quantum-mechanical calculations, indicated that electronegativity effects, bond angle changes, and π-electron overlap differences can all potentially contribute to ^{31}P shifts in a number of classes of phosphorus compounds. While these semiempirical isotropic chemical shift calculations are quite useful in providing a chemical and physical understanding for the factors affecting ^{31}P chemical shifts, they represent severe theoretical approximations.[68] More exact ab initio chemical shift calculations of the shielding tensor are very difficult and very few have been reported on phosphorus compounds.[68-70] Whereas calculations have largely supported the importance of electronegativity, bond angle, and π-electron overlap on ^{31}P chemical shifts, relating ^{31}P shift changes to structural and substituent changes must be approached with caution. Also, because ^{31}P shifts are influenced by at least these three factors, empirical and semiempirical correlations can only be applied to classes of compounds that are similar in structure. It should also be emphasized again, that structural perturbations will affect ^{31}P chemical shift *tensors*. Often variations in one of the tensor components will be compensated by an equally large variation in another tensor component with only a small net effect on the isotropic chemical shift. Interpretation of variations of isotropic ^{31}P chemical shifts should therefore be approached with great caution. Within these limitations, a number of semiempirical and empirical observations and correlations, however, have been established and have proved useful in predicting ^{31}P chemical-shift trends.[15] Indeed, unfortunately no single factor can readily rationalize the observed range of ^{31}P chemical shifts.

3. Bond Angle Effects

Several empirical correlations between ^{31}P chemical shifts and X–P–X bond angles have been noted.[71-74] Note that success here depends on the fact that these correlations deal with only a limited structural variation: in the case of phosphate esters, the number, and chemical type of R groups attached to a tetrahedron of oxygen atoms surrounding the phosphorus nucleus. As shown in Figure 2, bottom curve, for a wide variety of different alkyl phosphates (mono-, di-, and triesters, cyclic and acyclic neutral, monoanionic, and dianionic esters), at bond angle <108° Gorenstein[71] has shown that a decrease in the smallest O–P–O bond angle (obtained from X-ray data) in the molecule results in a deshielding (downfield shift) of the phosphorus nucleus. At bond angles >108°, deshielding of the ^{31}P nucleus occurs with further increase in bond angles.

Martin and Robert[75] have shown that a similar correlation of S–P–S bond angles and ^{31}P chemical shifts in 2-thioxo-2-*tert*-butyl-1,2,3-dithiaphospha compounds likely also exist (Figure 2, top curve). Contractor et al.[76] have observed a similar variation for PO_2N_2 tetrahedra, further confirming this bond-angle effect in tetracoordinated phosphorus compounds (middle curve; Figure 2).

Bond-angle changes and hence distortion from tetrahedral symmetry in tetracoordinated phosphorus should affect the chemical-shift anisotropy as well. Dutasta et al.[77] experimentally have verified this bond-angle effect in a solid-state ^{31}P NMR study on a series of cyclic thioxophosphonates. The shielding tensors are very sensitive to geometrical changes, and in fact, a linear correlation appears to exist between the asymmetry parameter η and the intracyclic bond angle α. The anisotropy is also correlated to the bond angle, whereas the average, isotropic chemical shielding shows a much poorer correlation.

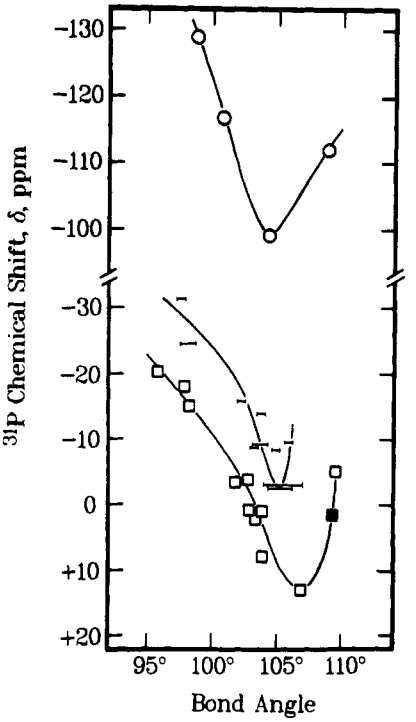

Figure 2. Phosphorus-31 chemical shifts of 2-thioxo-2-*tert*-butyl-1,3,2-dithiaphospha compounds vs S–P–S bond angle (O, upper left). Phosphorus-31 chemical shifts of PO_2N_2 tetrahedra vs bond angle (middle) derived from Martin and Robert[75] and derived from Contractor et al.[76] (|–|). Phosphorus-31 chemical shift of phosphate esters versus O–P–O bond angle (lower) derived from Gorenstein[71] (□) and Contracter et al.[76] (■). (Reprinted from ref 178. Copyright 1993 Marcel Dekker, Inc.)

The importance of the geometry about the phosphate tetrahedron in influencing ^{31}P chemical shifts is nicely illustrated in Figure 3. Using magic angle spinning, solid-state NMR, Cheetham et al.[60] have measured the ^{31}P shielding tensors, the chemical shift anisotropy, and the isotropic chemical shift (eqs 2 and 3) for various crystalline orthophosphates and higher phosphates. From the X-ray crystallographic structures of these same phosphates, they calculated the summed bond strengths at oxygen atoms, $\Sigma[S(O^{2-})]$, a term defined by Smith et al.,[78] and roughly related to P–O bond lengths. As shown in Figure 3 a reasonable correlation does appear to exist between the bond strengths at oxygen and isotropic ^{31}P chemical shifts. The isotropic chemical shift moves upfield as the bond strength at oxygen increases. It should be noted that the variation in the individual shielding tensors is considerably larger than the isotropic shielding.[60,78]

Gorenstein and Kar[79] have attempted to calculate the ^{31}P chemical shifts for a model phosphate diester in various geometries to confirm theoretically the bond-angle correlation. Using CNDO/2 SCF molecular orbital calculations, a correlation was drawn between calculated phosphorus electron densities and isotropic

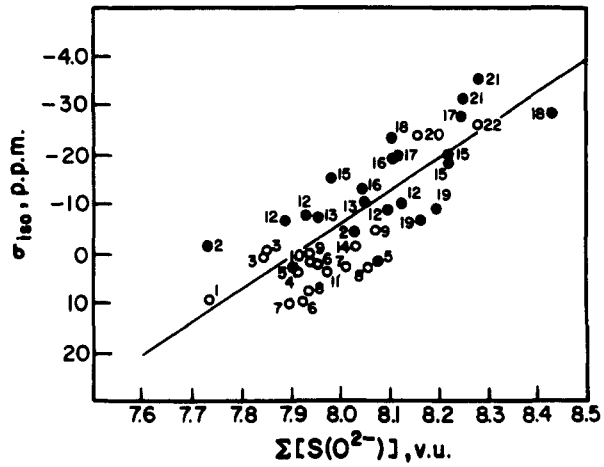

Figure 3. Plot of the summed bond strengths at oxygen (valence units, v.u.) following the method of ref 231 vs the ^{31}P magic angle spinning NMR isotropic chemical shifts, δ_{iso} (eq 2) relative to 85% H_3PO_4. Open and closed circles are metal (M) orthophosphates (such as $M_nH_{3-n}PO_4$) and metal higher phosphates (such as $M_nP_2O_7$), respectively. Numbering and actual structures may be found in ref 231. (Reprinted from ref 60. Copyright 1986 Chemical Society of London.)

^{31}P chemical shifts, and indeed deshielding of the phosphorus atom with decreasing O–P–O bond angles was found. A slightly better correlation was achieved between observed and calculated ^{31}P chemical shifts using both a Karplus–Das-type average excitation approximation semiempirical theoretical approach.[80]

4. Stereoelectronic Effects on ^{31}P Chemical Shifts

Semiempirical molecular orbital calculations[79] and ab initio gauge-invariant-type, molecular orbital, chemical-shift calculations[69,70] suggested that ^{31}P chemical shifts are also dependent on P–O ester torsional angles. The two nucleic acid P–O ester torsional angles, ζ and α are defined by the R–O–P–O(R′) dihedral angles (see Figure 1). These chemical-shift calculations and later empirical studies indicated that a phosphate diester in a B_I conformation (both P–O ester bonds gauche(–) or –60°) should have a ^{31}P chemical shift 1.6 ppm upfield from a phosphate diester in the B_{II} conformations (α = gauche(–); ζ = trans or 180°).[50,51] In the B_I conformation normally observed in the crystal and NMR structure of duplex B DNA, the phosphate is symmetrically disposed relative to the major and minor grooves. In the B_{II} state the phosphate is oriented more toward the minor groove.

As discussed in more detail in following sections analysis of ^{31}P chemical shifts and H3′-P coupling constants in nucleic acids have provided support for this stereoelectronic effect on ^{31}P shifts. If ^{31}P chemical shifts are sensitive to phosphate ester conformations, they potentially provide information on two of the most important torsional angles that define the nucleic acid deoxyribose phosphate backbone. Indeed following the original suggestion of Sundaralingam,[22] and on the basis of X-ray crystallographic studies of oligonucleotides, Saenger[29] has noted that the P–O bonds may be considered the "major pivots affecting polynucleotide structure". Although the two conformations have been observed crystallographically in nucleic acids,[81,82] there has been some controversy whether the B_{II} conformation exists in solution since there is some suggestion that some local conformational variations and B_I/B_{II} conformational differences arise from crystal packing effects.[83–85] It is here that ^{31}P NMR studies have proven so important.

5. Extrinsic and Other Effects on ^{31}P Chemical Shifts

Environmental effects on ^{31}P chemical shifts are generally smaller than the intrinsic structural effects. Lerner and Kearns[86] have shown the ^{31}P shifts of phosphate esters are modestly sensitive to solvent effects (varying as much as 3 ppm from 100% H_2O to 70% DMSO (H_2O)), and Costello et al.[87] have noted similar sensitivity of ^{31}P shifts of orthophosphate, diethyl phosphate, and monoethyl orthophosphate to high salt (0–5 M added salt). Gorenstein and coworkers[16,17,88] have noted that ^{31}P shifts are also sensitive to temperature, although they have analyzed this effect at least in part in terms of the stereoelectronic ^{31}P shift effect.

Under more modest changes in solvent and salt conditions, the intrinsic (and particularly stereoelectronic) effects appear to largely dominate ^{31}P chemical shifts of phosphate esters. Gorenstein and co-workers has used this relationship to probe the structure of nucleic acids.[1,7,12,15,17–19,88–90] Other possible factors that could affect ^{31}P shifts in phosphate esters have been found generally to be relatively unimportant. Thus ring-current effects associated with the bases in double helical nucleic acids are expected and found[20] to have only small (<0.1 ppm) perturbations on the ^{31}P signals. This diamagnetic contribution to the ^{31}P chemical shift influences ^1H and heavy-atom chemical shifts to the same extent and is strongly distance dependent. The phosphorus nucleus is shielded by a tetrahedron of oxygens, and therefore aromatic groups such as nucleic acid bases generally never approach close enough to cause any marked shielding or deshielding.

3. *Assignment of ^{31}P Signals of Oligonucleotides*

^{17}O-labeling methodologies were originally developed to assign the ^{31}P signals of the phosphates in a number of oligonucleotide duplexes[12,91–94] and polynucleotides.[95] However, the site-specific labeling of the monoesterified phosphoryl oxygens of the backbone with ^{17}O or ^{17}O-^{18}O methodology suffered by being both expensive and time consuming. Multidimensional ^{31}P–^1H NMR spectroscopy[13,94,96,97] has provided a convenient, inexpensive alternative for the assignment of ^{31}P chemical shifts in moderately sized oligonucleotides. Conventional 2D ^{31}P–^1H heteronuclear correlation (HETCOR) NMR spectroscopy has been applied with limited success to short oligonucleotides.[13,93] However, a ^{31}P–^1H long-range constant time HETCOR,[94,98] a 2D heteronuclear J cross-polarization heteroTOCSY,[99–103] a 2D heteronuclear TOCSY-NOESY,[104] a 2D TOCSY/^1H–^{31}P INEPT[99,105] and other indirect detection (^1H detection) HETCOR experiments[97,106] and HELCO experiments[107] have been successfully used to assign ^{31}P signals in 6–14 base-pair duplex DNA and RNA. A very nice 3D heteroTOCSY-NOESY experiment[108] has recently been developed which promises increased spectral dispersion by adding a third frequency dimension. This may prove

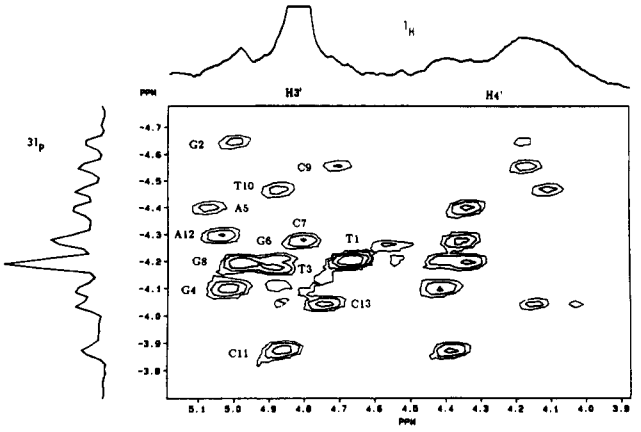

Figure 4. Pure absorption phase ^{31}P–^{1}H PAC spectrum of tetradecamer duplex d(TGTGAGCGCTCACA)$_2$, at 200 MHz (^{1}H). ^{31}P chemical shifts are reported relative to trimethyl phosphate which is 3.456 ppm downfield from 85% phosphoric acid. (Reprinted from ref 94. Copyright 1988 Academic.)

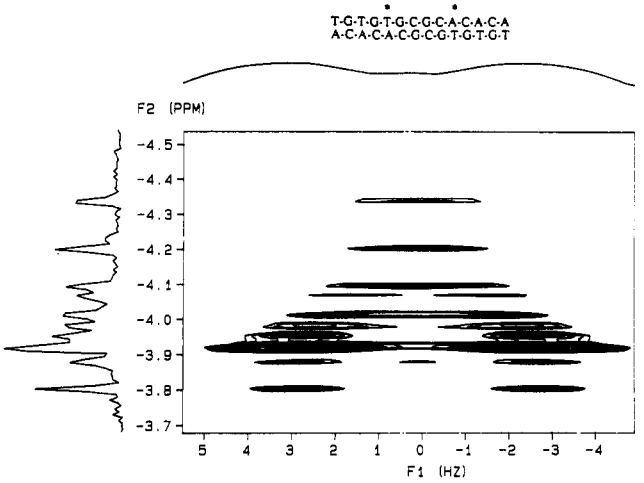

Figure 5. 2D ^{31}P–^{1}H J-resolved spectra at 200 MHz (^{1}H) of duplex 14-mer d(TGTGAGCGCTCACA)$_2$. The 1D decoupled ^{31}P NMR spectrum is also shown along one axis and the H3′ coupled doublets are shown along the second dimension. ^{31}P chemical shifts are reported relative to trimethyl phosphate. (Reprinted from ref 20. Copyright 1988 American Chemical Society.)

to be extremely valuable for ribooligonucleotides where very little ^{1}H spectral dispersion in the sugar protons is unfortunately observed.[104] Recent ^{15}N and ^{13}C labeling of oligonucleotides[109–111] hold promise for future assignment of ^{31}P signals for even larger nucleic acids and complexes.

For oligonucleotides longer than 4–5 nucleotide residues the simple heteronuclear correlation measurements suffer from poor sensitivity as well as poor resolution in both the ^{1}H and ^{31}P dimensions. The poor sensitivity is largely due to the fact that the ^{1}H–^{31}P scalar coupling constants are about the same size or smaller than the ^{1}H–^{1}H coupling constants. Sensitivity is substantially improved by using a heteronuclear version of the "constant time" coherence transfer technique, referred to as COLOC (*co*rrelation spectroscopy via *lo*ng range *co*upling) and originally proposed for ^{13}C–^{1}H correlations.[112] A pure absorption phase constant time (PAC) pulse sequence to emphasize ^{1}H–^{31}P correlations in oligonucleotides further improves sensitivity and resolution.[94] This pulse sequence incorporates both evolution of antiphase magnetization and chemical shift labeling in a single, "constant time" delay period, thereby improving the efficiency of coherence transfer and increasing sensitivity. The PAC sequence also gives homonuclear decoupling during t_1 and thus improves the resolution. For even more stringent heteronuclear correlations a *do*uble *c*onstant time (DOC) ^{1}H–^{31}P pulse experiment has also been developed.[98]

The PAC spectrum of the self-complementary 14 base-pair oligonucleotide duplex d(TGTGAGCGCTCACA)$_2$ is shown in Figure 4. The cross-peaks represent scalar couplings between ^{31}P nuclei of the backbone and the H3′ and H4′ deoxyribose protons. The chemical shifts of these protons are determined, as described above, by the sequential assignment methodology for B-DNA using the ^{1}H-^{1}H NOESY and COSY spectra. Assignment of the ^{31}P signal of the ith phosphate is achieved through connectivities with both the H3′(i) and H4′(i + 1) deoxyribose protons. (The ^{1}H chemical shifts are first assigned by 2D ^{1}H-^{1}H sequential assignment methodologies.[4,6,7,10,113]) Although the 5′H-(i + 1) and H5″(i + 1) protons overlap with the 4′ protons, the intensities for the ^{31}P-5′ and H5″ PAC cross-peaks generally appear to be much weaker than the H4′ cross-peaks. Similar behavior has been noted in ^{31}P-^{1}H HETCOR studies on other oligonucleotides[7,13,14,97,114] and presumably reflects the strong and large 5′ and 5″ coupling.

Indeed for modest size nucleic acids that are not in B- or A-form duplex geometries, the ^{31}P heteronuclear correlation spectra provide an important tool for ^{1}H sequential assignment. Thus, correlation between the 3′-proton of the ith residue and the 4′- (and possibly 5′, 5″-) protons of the i + 1 residue allow sequential assignment through coherence transfer methods rather than NOESY distance dependent correlations.[94,103,104] Again unfortunately with small ^{1}H–^{31}P couplings (≤10 Hz), for larger oligonucleotides (>30–40 residues) and with line widths often larger than the coupling constants, coherence transfer methods will generally fail because of poor sensitivity. Perhaps with ^{13}C labeling or even natural abundance, ^{13}C–^{31}P coherence transfer correlation methods will allow assignment for even larger nucleotides because C4′–P coupling constants between the i and i + 1 residues are generally around 9–10 Hz.[115]

4. ^{31}P Heteronuclear Coupling Constants

In order to establish a stereoelectronic factor contributing to the variation in ^{31}P chemical shifts of nucleic acids, it has proven to be critical to be able to measure the backbone torsional angles. Until recently, only the three bond $J_{H3'-P}$ coupling constants in oligonucleotide duplexes could be readily determined from the selective 2D J-resolved spectrum[116] such as that shown in Figure 5. Notice as shown in Figure 5 the very interesting pattern of monotonically decreasing coupling constants for the signals to higher field. This "Christmas tree"-shaped pattern is almost always observed in duplex oligonucleotides[20,116–120] and strongly supports a correlation between ^{31}P chemical shifts and $J_{H3'-P}$ coupling constants. This pattern collapses at higher temperatures, and at temperatures above the melting temperature of the duplex all of the coupling constants are nearly identical, $J_{H-P} \approx 8.0$–8.5 Hz.

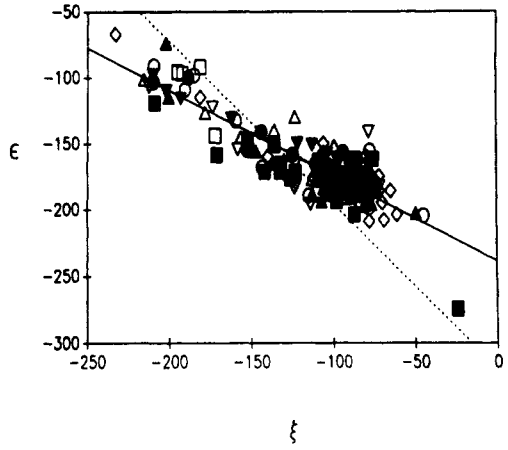

Figure 6. Plot of P–O3′ (ζ) vs C3′–O3′ (ϵ) torsional angles for individual phosphates of B-DNA crystal structures: (●) dCGCGAATTCGCG, room temperature;[232] (▲), dCGCGAATTCGCG, 16 K;[232] (▼), dCGCGAATTCGCG-*cis*-dichlorodiaminoplatinum(II);[232] (△), bent dCGCGAATT^{Br}CGCG;[232] (○) linear dCGCGAATT^{Br}CGCG;[232] (■) dCGCGAATTCGCG-Hoschst 33258;[233] (◇) dCGCGAATTTGCG;[234] (□) dCCAAGATTGG;[81] (▽) dGCGCGC.[81] The best straight (solid) line is $\zeta = -367.5 - 1.54\epsilon$ which differs slightly from that derived by Dickerson based upon just the four dodecamer structures (dashed line, $\zeta = -317 - 1.23\epsilon$). (Reprinted from ref 21. Copyright 1990 Adenine Press.)

The observed three-bond coupling constants can be analyzed with a proton–phosphorus Karplus relationship to measure the H3′–C3′–O–P torsional angle θ from which the C4′–C3′–O–P torsional angle ϵ ($= -\theta - 120°$) may be calculated. The relationship

$$J = 15.3\cos^2(\theta) - 6.1\cos(\theta) + 1.6 \qquad (4)$$

has been determined by Lankhorst et al.[121] As shown by Dickerson[27,28] there is a strong correlation ($R = -0.92$) between torsional angles C4′–C3′–O3′–P (ϵ) and C3′–O3′–P–O5′ (ζ) in the crystal structures of various duplexes (ζ may be calculated from the relationship:[27,28] $\zeta = -317 - 1.23\epsilon$).

The original correlation of ϵ and ζ torsional angles was based upon a limited comparison of several B-DNA crystal structures.[27,28] As shown in Figure 6, ϵ torsional angles were collected from 9 B-DNA crystal structures and plotted versus their corresponding ζ torsional angles.[21] Again, a strong correlation ($R = -0.86$, $\zeta = -348.11 - 1.42\epsilon$) exists between the two torsional angles, confirming the previous relationship (see also ref 122). Both B_I and B_{II} backbone conformations are observed in the B-DNA crystal structures as shown by the two relative clusters in the ϵ versus ζ plot of Figure 6. Thus both torsional angles ϵ and ζ can often be calculated from the measured P–H3′ coupling constant. When both ϵ and ζ can be separately measured (by X-ray or NMR restrained molecular dynamics calculations), the two states are best characterized by the value of $\epsilon - \zeta$ which has a value of ca. −90° or +90° for a B_I or B_{II} state, respectively. The α and γ torsional angles are also highly correlated in A-DNA, with a correlation coefficient also of −0.92[123] (β is contrained to a trans conformation in both B- and A-DNA).

A plot of observed ^{31}P chemical shifts and $J_{H3'-P}$ coupling constants is plotted in Figure 7.[118] In addition the Karplus relationship of eq 4 is also plotted. The Karplus relationship provides for four different torsional angle solutions for each value of the same coupling constant. Although all four values are shown in Figure 7, the limb which includes ϵ values between 0 and −270° is sterically inaccessible in nucleic acids.[29] Generally it is assumed that the coupling constants, which can vary only between 1 and 11 Hz, all correspond to ϵ torsional angles on a single limb nearest the crystallographically observed average for nucleic acids[29] ($\epsilon = -169 \pm 25°$). This need not always be true, especially since phosphate ester conformations corresponding to either of the other two solutions are observed crystallographically.[29] However, as shown in Figure 7, nearly all of the phosphates for normal Watson–Crick duplexes fall along only a single limb of the Karplus curve. Exceptions include several phosphates adjacent to some GA-mismatch duplexes.[124,125] In addition, it is quite interesting that the measured ^{31}P chemical shifts and coupling constants for the two phosphates at the site of a tetramer duplex actinomycin D drug complex do not fit on the main limb of the Karplus curve, although the values do nicely fit on the other two solutions of the curve (Figure 7). Indeed crystal structures[29] of related intercalator duplex complexes confirm that the phosphates often are constrained to conformations that best correspond to the other solutions. These intercalator drug duplex complexes quite generally show large downfield shifts of the ^{31}P signals (see section 7).[16,51,126]

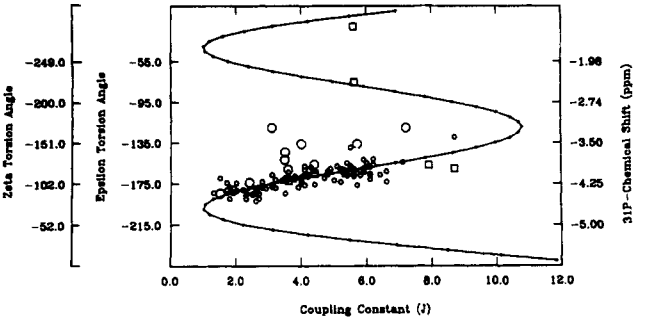

Figure 7. Plot of ^{31}P chemical shifts for the oligonucleotide sequences previously studied in our laboratory[20,118,184] (○) and the actinomycin-D bound d(CGCG)$_2$ tetramer complex[235] (□) with their measured $J_{H3'-P}$ coupling constants. (The ◯ data points correspond to phosphates in a tandem GA-mismatch decamer duplex[125] which shows unusual, slowly exchanging signals.) Also shown are the theoretical ϵ and ζ torsion angles (solid curve) as a function of coupling constant derived from the Karplus relationship (ϵ) and the relationship $\zeta = -317 - 1.23\epsilon$. ^{31}P chemical shifts are reported relative to trimethyl phosphate. (Reprinted from ref 125. Copyright 1990 American Chemical Society.)

In addition, perturbations in ^{31}P shifts can also arise from variations in the α (O3′–P–O5′–C5′) torsion angle that could also explain the "anomalous" behavior of those ^{31}P signals of phosphates which do not fall on the main limb of the Karplus curve. While the ζ torsional angle is found to be the most variable one in the B-form of the double helix, the other P–O torisonal angle, α, is one of the most variable in the A-form of the duplex.[29] The two points falling furthest off the main limb correspond to two phosphates in a 10-mer GA mismatch, d(CCAAGATTGG)$_2$.[125] The unusual geometry of the tandem mismatch could allow significant variation of the α (O3′–P–O5′–C5′) and β (P–O5′–C5′–C4′) torsional angles.

Unfortunately, the β torsional angles have in practice been generally unobtainable even in moderate length

duplexes. Selective 2D J-resolved spectra generally fail for H4′, H5′, or H5″ coupling to ^{31}P because the spectral dispersion between these protons is so limited. However, with either ^{13}C labeling or even natural abundance ^{13}C methods,[115,127] it is possible to measure not only the ^{1}H–^{31}P but also the ^{13}C–^{31}P coupling constants. Analysis of the 2D multiplet pattern, especially the "E COSY" pattern of the ^{1}H–^{13}C HSQC spectrum, has allowed extraction of many carbon (C3′, C4′, C5′) and proton (H3′, H4′, H5′, H5″) coupling constants to phosphorus.[115] As indicated earlier, C4′–P coupling constants for an octamer deoxyribonucleotide duplex are larger than ^{1}H–^{31}P coupling (varying from 18.5 to 21.7 Hz for the sum of the two coupling constants). This variation confirms the sequence-specific nature of the observed variation in the H3′–P coupling constants and in the future needs to be carefully explored. Unfortunately C4′ to ^{31}P connectivities between the i and $i+1$ residues are both 3-bond and therefore the coupling constants are of comparable value if the ϵ and β torsional angles are both ~180°. This appears to be true for several residues in the octamer. Interestingly several H5′–P coupling constants measured in the octamer varied between 2.8 and 4.0 Hz, suggesting that there is also some sequence-specific variation in the β torsional angle.

It is important to remember that ^{31}P chemical shifts are dependent on factors other than torsional angles alone. As noted above, ^{31}P chemical shifts are very sensitive to bond angle distortions as well.[15,71,128,129] It is quite reasonable to assume that backbone structural distortions as observed in mismatch duplexes, extrahelical base duplexes, or drug–duplex complexes also introduce some bond-angle distortion as well. Widening of the ester O–P–O bond angle indeed is expected to produce an upfield shift[15,71] while narrowing of this bond angle causes a downfield shift, and it is possible that this bond-angle effect could account for the anomalous shifts. Indeed very large ^{31}P chemical shift variations (ca. 7 ppm) are observed in tRNA phosphates,[130,131] and are likely due to bond angle distortions in these tightly folded structures.

By ignoring the drug–duplex points that fall off the main limb of the Karplus curve and by assuming a linear correlation between the coupling constants and ^{31}P chemical shifts (effectively a linear fit to the data on the main limb of the Karplus curve), the correlation coefficient is found to vary from −0.79 to −0.92 (at ambient temperature) for various oligonucleotide duplexes (the correlation coefficient for correlation of all of the main limb data is ca. −0.81).[20] Remarkably a linear correlation is even observed up to 80 °C.

Thus, for "normal" B-DNA geometries, there is an excellent correlation between the phosphate resonances and the observed torsional angle while phosphates which are greatly distorted in their geometry must be more carefully analyzed. Importantly, knowledge of both ^{31}P chemical shift and $J_{H3'-P}$ coupling constant can be very helpful in the proper interpretation of phosphate ester conformation.

Roongta et al.[118] have analyzed the variation in the ^{31}P chemical shifts and $J_{H3'-P}$ coupling constants (Figure 7) in terms of fractional populations of the two thermodynamically stable B_I and B_{II} states. From the crystal structure data, the average ϵ torsional angle value for the B_I state is −190° and for the B_{II} state is 105°.[27,28] These ϵ values approximate the maximum possible range of $J_{H3'-P}$ coupling constants (for $\epsilon = -105°$, $J_{H3'-P} = 10.0$ Hz and for $\epsilon = -190°$, $J_{H3'-P} = 1.3$ Hz). In addition in this torsional angle range, the Karplus curve is nearly a single-valued function. (Actually it is only single valued in the range of $\epsilon \approx -200$ to −120°; between −105 and −120°, the coupling constant is in the range of 10.0 − 10.8 Hz.) By assuming the measured coupling constant represents the weighted average of the coupling constants in the two states and by using the two extreme values of ϵ, the percentage B_I state can be estimated from the relationship

$$\%B_I = 100\% - \%B_{II} \sim \frac{J_{H3'-P}(\text{observed}) - J_{H3'-P}(-105°)}{J_{H3'-P}(-190°) - J_{H3'-P}(-105°)} \times 100\%$$

Under these assumptions and from the plot of Figure 7, the ^{31}P chemical shift and $J_{H3'-P}$ coupling constant of a phosphate in a purely B_I conformational state is estimated to be ca. −4.6 ppm and 1.3 Hz, respectively. Similarly the ^{31}P chemical shift and $J_{H3'-P}$ coupling constants of a phosphate in a purely B_{II} conformational state should be ca. −3.0 ppm and 10 Hz, respectively. The ^{31}P chemical shift difference between the B_I and B_{II} conformational states is thus estimated to be 1.6 ppm. It is thus extremely gratifying that the experimentally observed results fully support the original calculations and hypothesis that the ^{31}P chemical shift of a B_{II}-type phosphate ($\zeta = t$) is ca. 1.5 ppm downfield of a phosphate in a B_I conformation ($\zeta = g^-$).[15,16,79]

The largest coupling constant that is measured is ca. 7–8 Hz which represents a ζ angle of about −120°. Analyzing the coupling constants in terms of the fractional populations of the B_I and B_{II} states, phosphates with $J_{H3'-P}$ near this maximum value thus have nearly equal populations of the B_I and B_{II} states. At 80 °C, on the basis of the observed coupling constants, the B_I and B_{II} states are also approximately equally populated in the random coil single strand form of the oligonucleotides. This is quite reasonable because on the basis of molecular orbital calculations, the B_I phosphate ester conformation is estimated to be less than 1.0 kcal/mol lower energy than a phosphate in the B_{II} conformation.[18,132]

On the basis of ^{31}P relaxation studies[133] it has been suggested that only small amplitude internal motions of the phosphates in a drug oligonucleotide complex are possible. Analysis of ^{31}P relaxation of a small duplex suggests that the molecule behaves as a rigid rotor with little internal motion.[134] However, the elbow motion representing a B_I to B_{II} transition involves concerted torsion about both ζ and ϵ, and this transition will not dramatically alter the angle or distance between the phosphorus atom and the H3′ atom. Vectors between other nearest-neighbor protons will also not change much and therefore there will be an appearance of little internal motion as monitored by relaxation studies of phosphates.

The dispersion in the ^{31}P chemical shifts of regular oligonucleotides is thus likely attributable to different ratios of populations of the B_I and B_{II} states for each phosphate in the sequence. By assuming that only the staggered rotamers define stable conformations, the

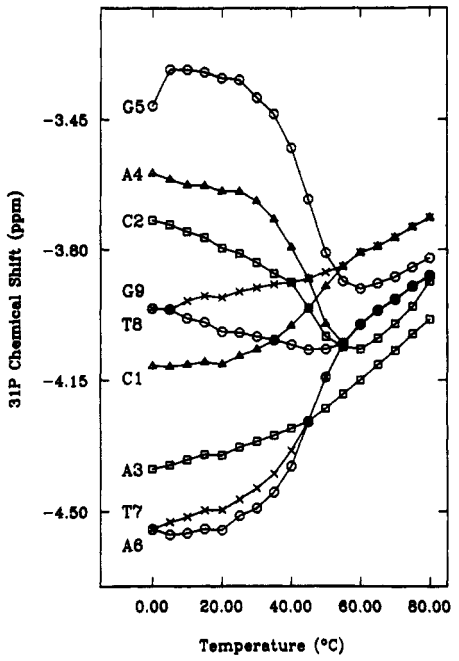

Figure 8. Temperature dependence of ^{31}P chemical shifts of GA-mismatch decamer duplex, d(CCAAGATTGG)$_2$. ^{31}P chemical shifts are reported relative to trimethyl phosphate. (Reprinted from ref 184. Copyright 1989 American Chemical Society.)

phosphate is assumed to make rapid jumps between the two states. Alternatively the phosphate could be considered to be constrained to a single intermediate P–O ester conformation. This later explanation appears to be ruled out by restrained molecular dynamics simulations[21] which clearly show that these intermediate conformational states are only transiently populated as the phosphate makes rapid jumps between the B_I and B_{II} states (see section 8). Thus the measured coupling constant appears to indeed reflect the populations of these two possible conformational states.

5. ^{31}P Melting Curves

The temperature dependence of ^{31}P chemical shifts and coupling constants provides an important monitor of both melting and premelting structural transitions in the phosphate ester backbone. Thus as represented by the ^{31}P chemical shift melting curve (Figure 8) for a tandem GA-mismatch decamer, d(CCAAGATTGG)$_2$,[125] there is a general downfield shift of many of the resonances with increasing temperature.[15,16] This is consistent with the change in the backbone conformation, generally B_I (g^- for P–O3′ ester bonds) in the duplex to a random mix of B_I and B_{II} conformations in the single-strand random coil. However, it is interesting to note that three of the peaks actually move considerably upfield beginning at about 30 °C. Two of these resonances, labeled G5 and A4, are connected to the 5′-oxygens of the mismatched base pairs. The inflection point in the curves for all phosphates occurs at ~40 °C corresponding to the T_m of the duplex. The coupling constants generally parallel the variation in ^{31}P chemical shifts and show quite similar melting curves.[118,125] Thus ^{31}P chemical shifts (and coupling constants) follow the expected variation in the sugar phosphate backbone conformation as the duplex melts into a random coil single strand.

6. ^{31}P NMR of Polynucleic Acids

^{31}P NMR may usefully be applied to the study of polynucleic acids as well.[49] As described above, the range of ^{31}P chemical shifts for individual phosphates in duplex fragments is <0.9 ppm. It is not surprising therefore that individually resolved signals are not observed for longer (>100 bp) nucleic acid fragments, for which much broader lines are expected. Infavorable circumstances, however, separate signals may be resolved.

Thus sonicated poly(A)·poly(U) ^{31}P spectra show two equal intensity signals separated by ca. 0.4 ppm (–1.2 and –1.6 ppm relative to 85% H_3PO_4). As shown by Alderfer and Hazel,[135] these signals are associated with the duplex. The chemical shifts of the triplex are +0.07, –0.38, and –0.90 ppm[135] referenced to 85% phosphoric acid. Joseph and Bolton[95] have shown by ^{17}O labeling of the phosphates that the two main ^{31}P signals are associated with phosphates in alternating conformations along the duplex poly(A)·poly(U) rather than the phosphates in the two different strands. The separation of the two signals could possibly be attributed to an "alternating A-RNA" structure.

The ^{31}P spectrum of poly[d(AT)] also gives two signals separated by as much as 0.8 ppm depending upon salt conditions.[136] In low-salt solution poly[d(AT)] shows a separation of ^{31}P signals of 0.24 ppm.[136] By thiophosphoryl labeling, Eckstein and Jovin[137] were able to establish that the deshielded ^{31}P signal arises from the TpA phosphates, which based upon an X-ray crystal model, are in a more extended trans-like, B_{II} phosphate ester conformation. The ^{31}P signal of the ApT phosphates is quite similar to that of a normal B-DNA phosphates and indeed is in a g^-,g^- B_I conformation.

One of the earliest, most direct indications that ^{31}P chemical shifts were dependent on phosphate ester conformations comes from the study of poly[d(GC)] and shorter oligomeric GC and related base duplexes. In high salt, the ^{31}P spectra of these alternating duplexes (including an RNA duplex) shows two signals of equal area with a chemical shift difference of 1.4–2.0 ppm.[138-142] The crystal structures of this high-salt left-handed Z-DNA conformation show an alternation along the sugar phosphate backbone (α, ζ) of either B_I-like (g^+,g^+ for CpG) and B_{II}-type (g^+,t or g^-,t for GpC) phosphates.[143-145] Sklenar and Bax[146] have nicely used the 2D heteronuclear indirect detection experiment to assign the downfield shifted signal to the B_{II} type of phosphates.

7. ^{31}P NMR of DNA–Drug Complexes

Patel[126,147] first reported that the intercalating drug, actinomycin D (Act D) shifted several phosphate diester signals up to 2.6 ppm downfield from the double helical signal upon binding to oligonucleotide duplexes containing dGdC base pairs. Thus, downfield shifts of 1.6 and 2.6 ppm in the dCdGdCdG–Act D (2:1) and 1.6 ppm in the pdGdC–Act D (2:1) complex at 8 °C have been observed. Similar shifts are also observed in other Act D oligonucleotide duplex complexes (cf refs 148 and 149).

These shifts are consistent with the Jain and Sobell[150] model for these intercalated complexes: partial un-

winding of a specific section of the double helix allows these planar, heterocyclic drugs such as Act D to stack between two base pairs. The downfield shifted peak in a $d(AGCT)_2$–Act D complex has been assigned to the dGdC base pair by the $^{17}O/^{18}O$ phosphoryl labeling method;[151] (see also ref 91). X-ray studies on various intercalating drug–duplex complexes[29,152] suggest that the major backbone deformation of the oligonucleotide upon intercalation of the drug involves changes in both the P–O and C–O torsional angles.

Similar spectral changes have been observed for drug–polynucleic acid complexes. For example, titration of the poly(A)·poly(U) ^{31}P spectra with ethidium produces a new signal 1.8–2.2 ppm downfield from the duplex signal.[153] At saturating levels of the drug ([drug]/[DNA] ratios > 0.5) the relative intensities of the downfield signal relative to the largely unperturbed upfield signal is ca. 1:1.

This deshielding for approximately one-half of the phosphate signals in the poly(A)·poly(U)·drug complexes is entirely consistent with the intercalation perturbation of the phosphate ester geometry observed in the Act D and related ethidium ion complexes. The chemical shift of this downfield peak is supportive of the intercalation mode of binding, since the purely electrostatic association between drugs and nucleic acid produces only small and generally upfield ^{31}P shifts.[154,155] The largely unperturbed upfield signals at 15 °C in these complexes likely represent undistorted B_I phosphates in regions adjacent to the intercalation site. The ca. 1:1 relative intensity of the downfield and main upfield peaks at saturating drug ratios is consistent with the nearest-neighbor exclusion model for these drug–duplex complexes. Thus at saturating drug ratios only every other base-pair step can accommodate an intercalated drug. The phosphate ester backbone at the intercalation site is in an extended conformation (see below), whereas the phosphate ester backbone at the two neighboring sites is in a normal B-DNA conformation.

In contrast to the above RNA duplex results, Wilson et al.[155,156] and Lai and Gorenstein[157] did not observe a separate downfield peak in the binding of ethidium, quinacrine, daunomycin, and tetralysine to sonicated DNA. In ^{31}P NMR studies on the intercalating drug–DNA complexes, increasing amounts of drugs only produces downfield shifts and line broadening. The difference between the duplex RNA and DNA systems is attributed to the rate of chemical exchange between the duplex–drug complex. In the drug–DNA complexes, the phosphates are undergoing fast chemical exchange between sites not involving the intercalated drug (nearest neighbor or further removed) and sites directly linking the intercalated base pairs.

The ^{31}P chemical shifts of various drug complexes[155,157] appear to correlate with the observed degree of unwinding of the duplex DNA upon drug binding (Figure 9). The helical twist values for various drug complexes that are used in Figure 9 represent the difference between the normal B-DNA helical twist angle of 35.6° and the observed helical unwinding angle resulting from binding of the drug. Because of the nearest-neighbor exclusion principle, at saturating concentrations of these drugs, only every other site has a bound drug. Because of fast chemical exchange

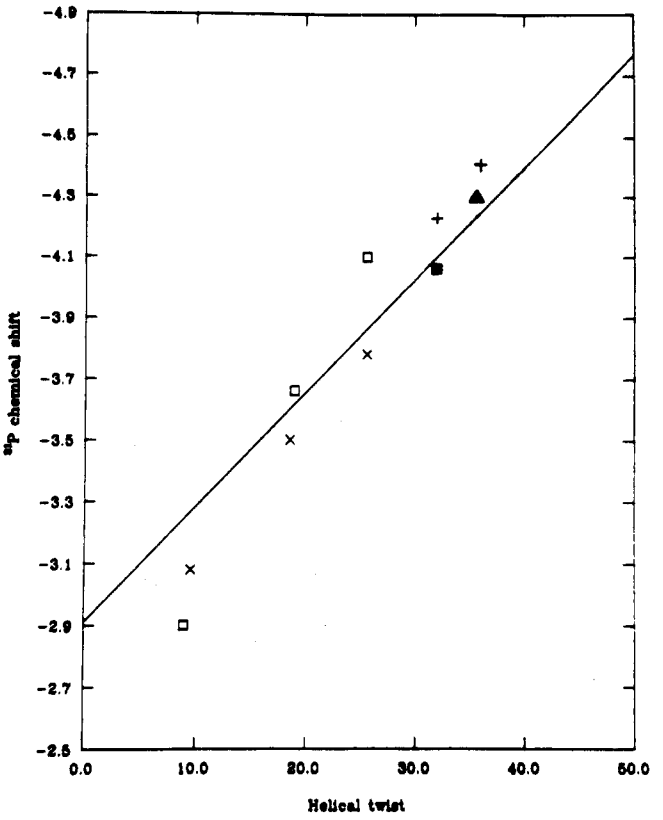

Figure 9. Plot of ^{31}P chemical shift vs calculated helix twist, t_9; 10–14 bp oligonucleotide terminal phosphate shifts (○; t_g derived from $t_g = 35.6 + 2.1\Sigma_1$)). Wilson and Jones'[155] drug–DNA data (×), drug–calf thymus DNA data[157] (□), A-DNA (■), B-DNA (△), and alternating poly[d(AT)] (+) shifts are shown. The helix twist for the drug–DNA is calculated from the difference between the helix twist of B-DNA ($t_g = 35.6°$) and the unwinding angle, ϕ for the drug–DNA complex (for ethidium ($\phi = 26°$), quinacrine ($\phi = 17°$), and daunomycin ($\phi = 10°$). The ^{31}P chemical shifts of the drug–DNA complexes have been corrected for chemical shift averaging. ^{31}P chemical shifts are reported relative to trimethyl phosphate. (Derived from ref 157).

averaging, only one ^{31}P signal is observed in these drug complexes and this must represent an average of the ^{31}P chemical shifts of phosphates at nonintercalative and intercalative sites. Correction for this chemical exchange averaging has been made in Figure 9 by multiplying the observed perturbation of the ^{31}P shifts by 2.

8. Sequence-Specific Variation in ^{31}P Chemical Shifts and Coupling Constants of Duplex Oligonucleotides

A number of "modest"-sized oligonucleotide sequences have had individual ^{31}P resonances completely assigned. ^{31}P chemical shifts of individual phosphates for similar sequences are quite similar and perturbations in the shifts are largely localized near the sites of base-pair substitution. While "complementary" phosphates (phosphates opposite each other on complementary strands) are chemically and magnetically nonequivalent, rather surprisingly, the ^{31}P chemical shifts at complementary phosphate positions generally follow the same pattern in both strands of the duplex regardless of base sequence or position, suggesting that the phosphate geometry is nearly the same in comple-

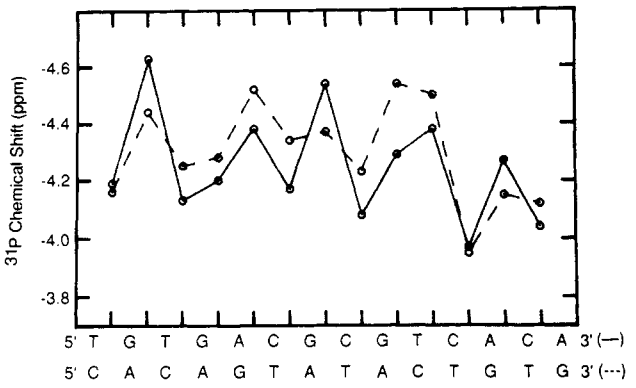

Figure 10. Comparison of the ^{31}P chemical shifts of tetradecamers, d(TGTGACGCGTCATA)$_2$ (solid line) and d(CACAGTATACTGTG)$_2$ (dashed line) vs sequence. ^{31}P chemical shifts are reported relative to trimethyl phosphate. (Reprinted from ref 158. Copyright 1989 American Chemical Society.)

mentary positions along both strands.[158] This suggests that local helical parameters which are symmetric across the base step (e.g. helix twist and roll)[29] but not tilt are largely responsible for the phosphate ester geometry changes.

A very intriguing comparison[158] of the ^{31}P chemical shift of two 14-mers, d(TGTGACGCGTCATA)$_2$ and d(CACAGTATACTGTG)$_2$, is shown in Figure 10. The two 14-mers are related by an "opposite" nucleotide sequence (a pyrimidine is replaced by the other pyrimidine and a purine is replaced by the other purine). This retains the purine–pyrimidine base steps but obviously completely alters the sequence at every position. As shown in Figure 10, remarkably, the pattern of variation of ^{31}P chemical shifts of the two sequences 14-mers are quite similar. The observed variation of ^{31}P chemical shifts is largely a function only of the purine–pyrimidine sequence. The through-space magnetic or electric chemical shielding effects of either a guanosine or adenosine base (i.e., through ring-current and electric charge effects) will not be identical at the phosphorus nucleus. The fact that it is immaterial whether an A or a G base is present at a particular purine position in the sequence, further supports the hypothesis that conformational differences are responsible for the ^{31}P chemical shift variations.

As pointed out in Ott and Eckstein[159] and Schroeder et al.[7,12] ^{31}P chemical shifts appear to vary in response to local, sequence-specific, and induced environmental distortions in the duplex geometry. Earlier attempts in the laboratory of Gorenstein and that of F. Eckstein utilized a set of simple "Calladine rules" to predict local helical structure. Thus Dickerson and co-workers[160] had shown that the helical distortions observed in the crystal structure of a dodecamer could be quantitatively predicted through a series of simple "Calladine rule" sum function relationships.[161] This was attributed to local helical variations introduced to relieve purine–purine steric clash in PyPu sequences. Other explanations for this variation have been offered, including intrinsic stacking interactions resulting from the differing charge distributions in the bases.[162] On the basis of the ^{31}P assignments of over a dozen oligonucleotides, Gorenstein et al. were able to establish a modest correlation between ^{31}P chemical shifts and the Calladine helical twist sum function for a number of the oligonucleotides.[7,12,20,157] The correlation coefficient (R) between ^{31}P shifts and helical twist was 0.71 if just the terminal phosphates and the ^{31}P chemical shifts of the drug complexes described in the previous section were included in the correlation. However in the middle region of the duplex oligonucleotides, no correlation (R = 0.05) was found between ^{31}P chemical shifts and helix twist.[20]

It is now becoming clear that the failure to observe a correlation between ^{31}P chemical shifts of duplex oligonucleotides and these sequence-specific local helical structural "Calladine rules" as derived from X-ray crystal structures simply reflect the failure of the rules themselves to accurately predict the solution-state sequence-specific local helical structural variations.[21,50,81,162,163–167] Further, NMR studies have suggested that the duplex conformation in solution may not be identical to the static picture provided by X-ray diffraction in the crystal state,[97,168] as one might expect. Fortunately 2D NOESY NMR solution structural methods are now sufficiently advanced that it is possible to determine some of the torsional angles and local helical structural parameters with reasonable precision and accuracy,[169,170] and now comparisons may be made between the solution conformation and ^{31}P spectra.

1. ^{31}P Chemical Shifts as a Function of Sequence and Position

Besides this sequence-specific effect, the ^{31}P chemical shifts of the phosphates generally move upfield as the position of the phosphate moves toward the center of the helix.[20,118] As mentioned above, one of the factors that will affect ^{31}P chemical shifts is the degree of conformational constraint imposed by the duplex geometry.[16,171,172] Base pairs closer to the ends of the duplex are less constrained to the stacked, base-paired geometry. This "fraying" at the ends imparts greater conformational flexibility to the deoxyribose phosphate backbone, and thus phosphates at the ends of the duplex will tend to adopt more of a mixture of different conformations. Phosphates located toward the middle of a B-DNA double helix assume the lower energy, stereoelectronically[18] favored polymer B_I conformation, while phosphodiester linkages located toward the two ends of the double helix tend to adopt a mixture of B_I and B_{II} conformations, where increased flexibility of the helix is more likely to occur. Because the B_I conformation is responsible for a more upfield ^{31}P chemical shift, internal phosphates in oligonucleotides would be expected to be upfield of those nearer the ends. Although several exceptions have been observed, this positional relationship appears to be generally valid for oligonucleotides where ^{31}P chemical shift assignments have been determined.[7,12,17,89,171,173] This "positional" ^{31}P chemical shift is superimposed on site- and sequence-specific effects.[7,12,20,171,172]

As shown in Figure 9 ^{31}P chemical shifts are sensitive to the degree of helix twist in various drug–DNA complexes. This (as well as other site- and sequence-specific effects in normal oligonucleotides) is very likely due to the changes in the length of the sugar–phosphate backbone which in turn alters the phosphate conformation. These local helical changes (and in the case of drug–DNA complexes, the additional structural changes incurred as the result of drug intercalation) require

changes in the deoxyribose phosphate backbone angles α and ζ (Figure 1). As the helix winds or unwinds or adjusts to accomodate an intercalated drug, the distance between the adjacent C-4′ atoms of deoxyribose rings along an individual strand must change to reflect the stretching and contracting of the deoxyribose phosphate backbone between a base step. To a significant extent, these changes in the overall length of the deoxyribose phosphate backbone "tether" in changes in the P–O ester (as well as other) torsional angles.[20] The sequence-specific variations in the P–O (and C–O) torsional angles may provide the linkage between the sequence-dependent structural variations in the duplex and ^{31}P chemical shifts. The similarity of the shift and coupling constants for complementary phosphates (Figure 10) suggests that local helical parameters which will symmetrically modulate the length of the sugar phosphate tether equally across the two strands in a base step are largely responsible for these changes (e.g. helix twist and roll[174]). However, large values of tilt (wedging along the long axis of the stacked base pairs) would create unequal tether lengths and hence differing ^{31}P shifts and coupling constants.

Analysis of the X-ray crystal structures[27-29] and NOESY distance refined structures[26] of B-form oligodeoxyribonucleotides has shown that torsional angles α, β, and γ on the 5′-side of the sugar are largely constrained to values $g^-(-60°), t(180°), g(+60°)$, whereas significant variations are observed on the 3′-side of the deoxyribose phosphate backbone. The greatest variation in backbone torsional angles is observed for ζ (P–O3′) followed by ϵ (C3′–O3′) and then δ (C4′–C3′). It is important to note that many of these torsional angle variations are correlated.[20,27-29]

As indicated previously, when the P–O3′ conformation is g^-, invariably the C–O3′ conformation (ϵ) is found to be t. This ϵ (t), ζ (g^-) conformation is the most common backbone conformation. In this B_I (t,g) conformation (Figure 1), δ can vary considerably (δ largely reflects the sugar pucker).[27,28] As δ increases to its maximum limit of ~160° in order to relieve any additional local helical distortion, ζ now begins to vary from −60° to −120° while ϵ largely remains fixed at trans.[27,28] At a maximal value for δ the phosphate ester conformation can switch to the B_{II} state ($\zeta = t$, $\alpha = g^-$; Figure 1). It is largely this variation in δ, ϵ, and ζ that allows the sugar phosphate backbone to "stretch" or "contract" to allow for sequence-specific variations in the local base-pair geometry of B-DNA. The B_I and B_{II} states represent ground-state minima with the P–O and C–O torsional angles in the staggered conformations.[132,175] Partially or fully eclipsed conformations which are not energy minima are only accessible through libration in each of the staggered states or through transient passage during the rapid jumps between the two ground states.

Thus the possible basis for the correlation between helix unwinding (helix twist) and ^{31}P chemical shifts in both nucleic acids and nucleic acid–drug complexes can be analyzed in terms of sugar phosphate backbone distortions.[20] Presumably, as the helix unwinds upon binding an intercalating drug, the length of the sugar phosphate backbone increases to accommodate the additional heterocycle intercalated between the two stacked base pairs with a base to base separation now of ~6.7 Å. This local helical unwinding and lengthening of the tether requires an increase in the population of the B_{II} conformation and shifts the ^{31}P signal downfield. However, as noted below, a different backbone readjustment occurs for changes in helix twist in normal B-type DNA.

2. Conformation and Dynamics of the Phosphate Ester Backbone

Unfortunately, ^{1}H–^{1}H 2D nuclear Overhauser effect spectra (NOESY) give no direct information on the phosphate ester conformation and NOESY distance-constrained structures have been suggested to be effectively disordered in this part of the structure.[26] However, as described above ^{31}P chemical shifts and ^{1}H–^{31}P coupling constants clearly indicate sequence-specific variations in the backbone conformation. The solution structural refinements of a d(CGCTTAAGCG)$_2$ decamer duplex, tandem-GA-mismatch decamer, and several tetradecamers[168,176-178] by a hybrid matrix/NOESY distance-restrained molecular dynamics methodology[50,168,179-181] provided important suggestions that full analysis of DNA structure requires a complete picture of the internal dynamics.

An example of an NMR-restrained molecules dynamics trajectory (time course) of the variations in the six backbone torsional angles, α–ζ of one internucleotide linkage in d(CGCTTAAGCG)$_2$ decamer duplex, is shown in Figure 11A–F.[21] Most of these torsional angles showed relatively small amplitude fluctuations about the average B-DNA values for the 50 ps restrained molecular dynamics calculation. As noted above in B-DNA the ϵ and ζ torsional angles show the largest variability and indeed our calculations demonstrate that large amplitude fluctuations occur for these two torsional angles. These torsional angle changes reflect a transition from the low-energy B_I conformation to the higher energy B_{II} conformation. These transitions were short lived and relaxed back to the low energy conformation. Other internucleotide phosphates show similar transitions (Figure 11G–L; only the ϵ and ζ torsional angles for three phosphates are shown), although the fraction of B_I/B_{II} states varies. Note how phosphate 8 (Figure 11, parts I and J) spends most of its time in the B_I conformation while phosphate 9 is largely dominated by B_{II}. These calculations also provided strong support for the coupled elbow conformational transition between the B_I and B_{II} conformations and the strong correlation between the ϵ and ζ torsion angles observed in the X-ray crystal structures of B-DNA.[27,28] The correlation between the ϵ and ζ torsion angles over the entire 50 ps restrained MD time course for the A17 phosphate on the 3′-strand of the decamer is shown in Figure 12. The similarity between the plots of Figure 6 (based upon the crystal structures) and 12 (based upon the solution structure derived from NOESY restrained MD calculations) is particularly striking and further supports the correlated motion.

There is some question whether some of the sequence-specific structural variations observed in the X-ray crystallographic studies are the result of less profound crystal packing forces.[83,84] Indeed Dickerson et al.[84] have suggested that all of the sequence-specific variation in the B_I and B_{II} conformations arises from crystal

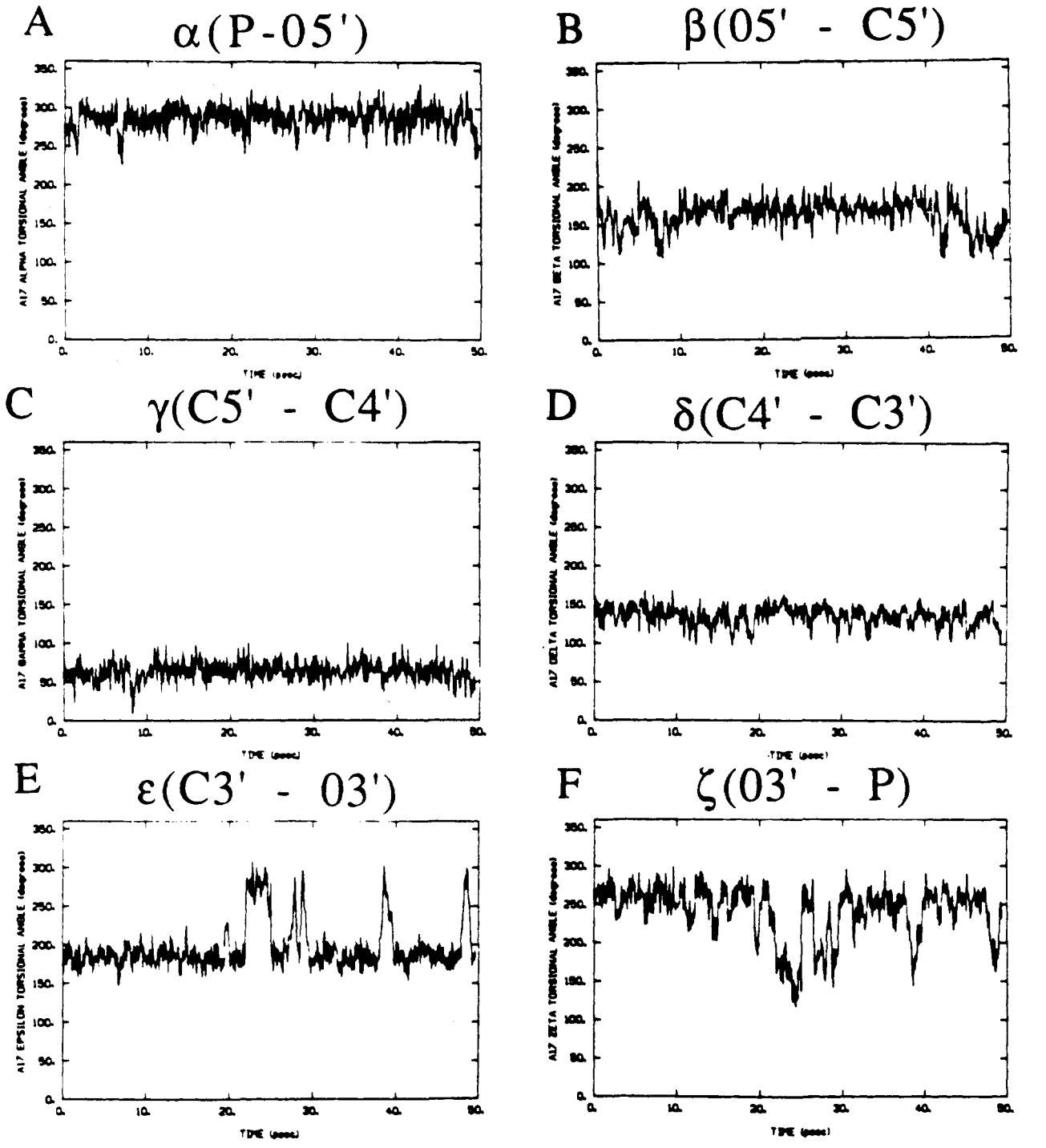

packing forces. Similar conclusions have been reached in a Raman spectroscopy analysis of the backbone phosphate conformation in solution and the solid state.[182] Our own results clearly show that there are significant variations (sequence- and/or position-dependent) in the relative populations of the B_I and B_{II} conformations in duplex oligonucleotides in solution. In the Dickerson et al.[84] analysis variation in local helix parameters such as helix twist, base roll, propeller twist, and sugar pucker are determined by base sequence and thus are "hard" parameters and a real phenomenon. They further argue that the backbone conformation is a "soft" parameter that is easily perturbed by crystal packing forces and is "an epiphenomenon". However in solution, the backbone conformation clearly does display sequence, position, and site specificity[20,118,158] and as such these variations indeed represent true "phenomena".

3. Origin of Sequence-Specific Variation in the ε and ζ Torsional Angles and P–H3′ Coupling Constants; C4′–C4′ Interresidue Distances

In normal DNA as the helix unwinds (and the helix twist t_g decreases), the length of the deoxyribose phosphate backbone decreases.[20,158,178] As in the case of the drug–duplex complexes, these local helical changes require changes in the deoxyribose phosphate backbone angles α and ζ. Yanagi et al.[183] pointed out the importance of the variations in the sugar phosphate backbone and the limitations it imposes on local helical parameters. Indeed it is possible that the failure of the

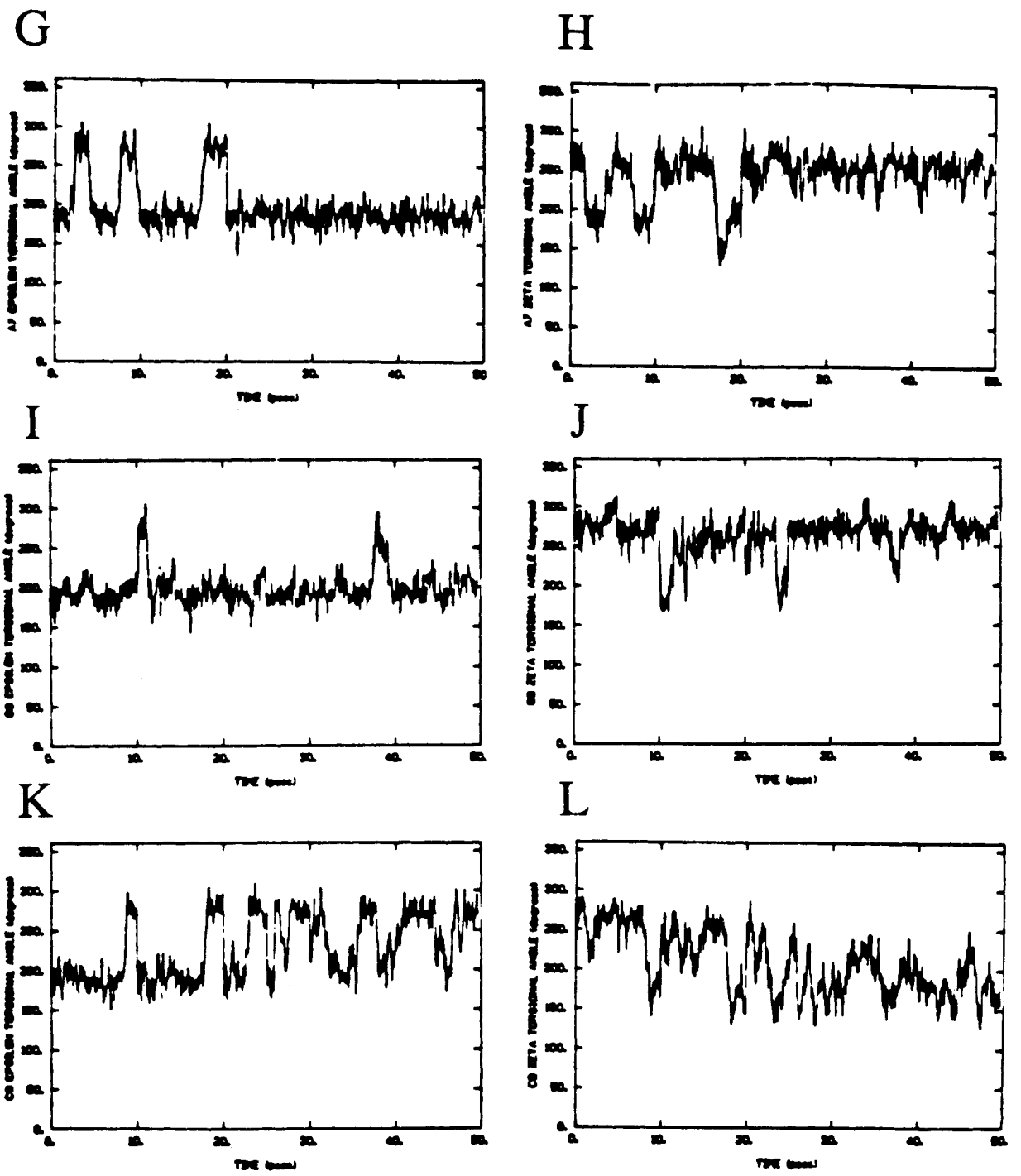

Figure 11. Time course for the fluctuations in the backbone torsional angles for the A17 residue of the d(CGCTTAAGCG)$_2$ decamer duplex during the restrained molecular dynamics refinement: (A) α, (B) β, (C) γ, (D) δ, (E) ϵ, and (F) ζ; (G–L) time course for only the ϵ (left panels) and ζ (right) panels for phosphates 7 (top), 8 (middle), and 9 (bottom) of the decamer. (Reprinted from ref 21. Copyright 1990 Adenine Press.)

Calladine rules to reliably explain the sequence-specific local helical structural variations is at least partially attributable to the failure to properly take into account this structural feature. The maximal length of the sugar phosphate backbone (in an all-trans conformation about each of the backbone bonds) is 7.4 Å, leading to a maximal C1′ to C1′ distance between adjacent sugars of 5.6 Å (Dickerson defines this as D_{xyz}).[183] The mean D_{xyz} found in crystals is 5.0 Å and thus the backbone is 90% extended. The observed range of D_{xyz} in crystals varies from 4.3 (77%) to 5.5 Å (98%). As earlier noted in ref 20 and further by Yanagi et al.[183] the backbone linkage (as measured by either the C4′–C4′ distance in Gorenstein's laboratory or Dickerson's C1′–C1′ distance) provides a connection between various local helical parameters such as rise, twist, and roll. It again supports the importance of the sugar phosphate conformation in helping to define or at least constrain the duplex base-pairing geometry.

Thus the distance between the adjacent C-4′ atoms of deoxyribose rings along an individual strand ($D_{4'4'}$) may be used as a measure of the overall length of the deoxyribose phosphate backbone "tether". Significantly, the $D_{C4'C4'}$ distances obtained from the four crystal structures[27-29] of the dodecamer duplex d(CGCGAATTCGCG)$_2$ as well as the calculated $D_{C4'C4'}$ dis-

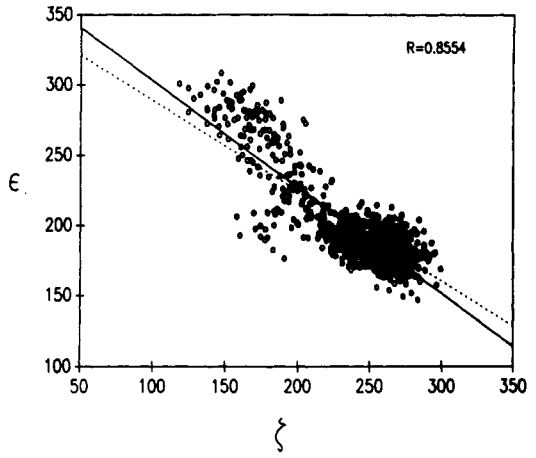

Figure 12. Plot of P–O3′ (ζ) vs C3′–O3′ (ϵ) torsional angles for the A17 residue of the d(CGCTTAAGCG)$_2$ decamer duplex during the last 45-ps restrained molecular dynamics refinement. ζ/ϵ torsional angles were obtained for the phosphate every 50 fs. The best straight (solid) line is $\zeta = -348.1 - 1.42\epsilon$ (R = 0.86). The dashed line is derived from the crystal structures from Figure 6 ($\zeta = -367.5 - 1.54\epsilon$). (Reprinted from ref 21. Copyright 1990 Adenine Press.)

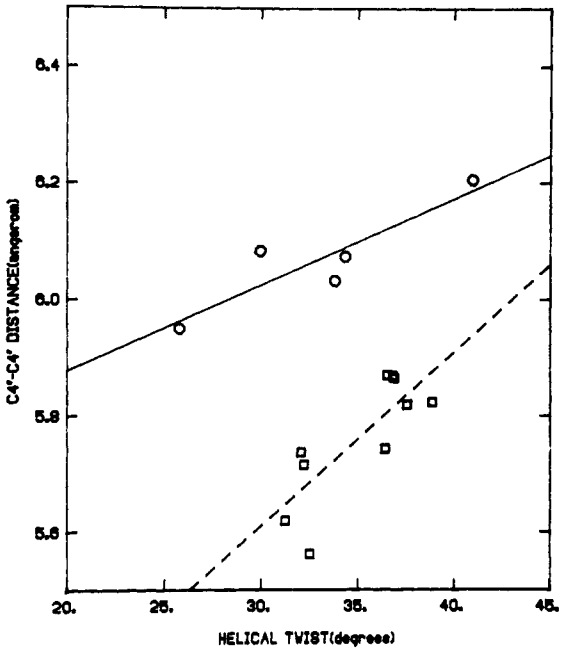

Figure 13. Correlation of distance between adjacent deoxyribose C4′ atoms, $D_{C4'C4'}$, along one strand of duplex oligonucleotide d(CGCTTAAGCG)$_2$ and helical twist parameter t_g derived from the solution structure for the decamer (O; solid line) and the crystal structures of the dodecamer d(CGCGAATTCGCG)$_2$ (□, dashed line). Values for the decamer were derived by averaging the entire last 45-ps time course for the restrained molecular dynamics refinement. The crystallographic data only includes B_I conformations and the residue at the ends of the duplex has been eliminated. Each conformation represents the average of phosphate conformations on complementary strands and has also been end for end averaged. (Reprinted from ref 21. Copyright 1990 Adenine Press.)

tances of the d(CGCTTAAGCG)$_2$ decamer also follow a similar change as a function of t_g, as shown in Figure 13.[21] The correlation coefficient between the crystallographically derived $D_{C4'C4'}$ distances and t_g is 0.77 (Figure 13). While the restrained MD calculated distances for the d(CGCTTAAGCG)$_2$ decamer duplex are shifted slightly from the crystal structure distances,

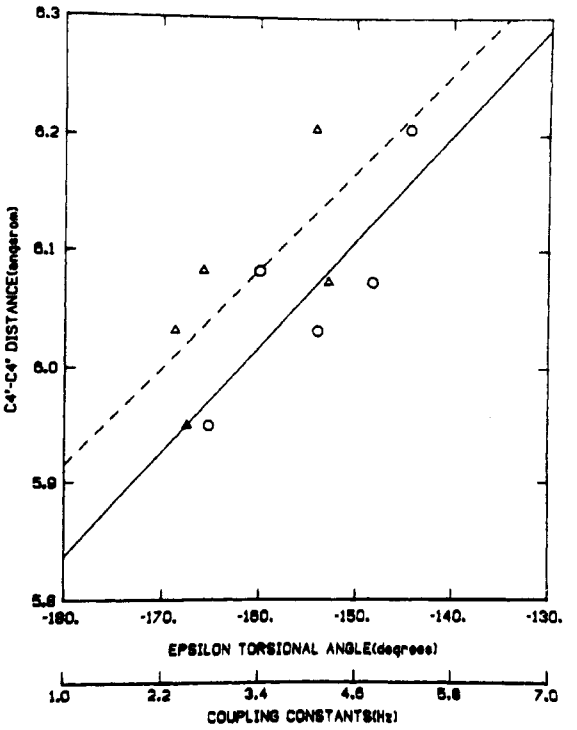

Figure 14. Plot of distance between adjacent deoxyribose C4′ atoms, $D_{C4'C4'}$, along one strand of the d(CGCTTAAGCG)$_2$ decamer vs measured P-H3′ coupling constant (Δ, dashed line) and the calculated ϵ torsional angles (O, solid line) derived by averaging the entire last 45-ps time course for the restrained molecular dynamics refinement for the decamer d(CGCTTAAGCG). (Reprinted from ref 21. Copyright 1990 Adenine Press.)

the trend is quite similar and the correlation is very good (R = 0.90).

A remarkable, similar correlation also exists between the $J_{H3'-P}$ coupling constant and the calculated C4′–C4′ distances derived from the NOESY distance-restrained MD-refined structure for the decamer (R = 0.69; Figure 14). Figure 14 also demonstrates that there is a good correlation between the derived ϵ torsion angles from the NMR/MD refinement and C4′–C4′ distances (R = 0.83). It is important to note that the ϵ torsional angles have been calculated by averaging all of the values taken every 50 fs in the entire last 45 ps NOESY distance-restrained MD refinement.

4. ^{31}P NMR Spectra of a Tandem GA-Mismatch Duplex, d(CCAAGATTGG)$_2$

A tandem GA-mismatch decamer, d(CCAAGATTGG)$_2$ has provided additional insight into the role of phosphate ester conformation and backbone dynamics on ^{31}P NMR chemical shifts and coupling constants.[184] The ^{31}P spectrum is quite dispersed at 20 °C with a range of 1.2 ppm. This "spread" in chemical shifts is unusual for a duplex DNA fragment, most being generally less than 0.7 ppm. Even in the cases where there are two mismatch sites (nontandem), the chemical shifts of the ^{31}P spectrum are dispersed between 0.5 and 0.9 ppm.[118,185-187] In the GA mismatch two low-field signals are separated from the main cluster representing more normal type of phosphates (Figure 8). These unusual ^{31}P signals are associated with phosphates at or near the site of the mismatch (much as is found in drug–DNA complexes). While it may

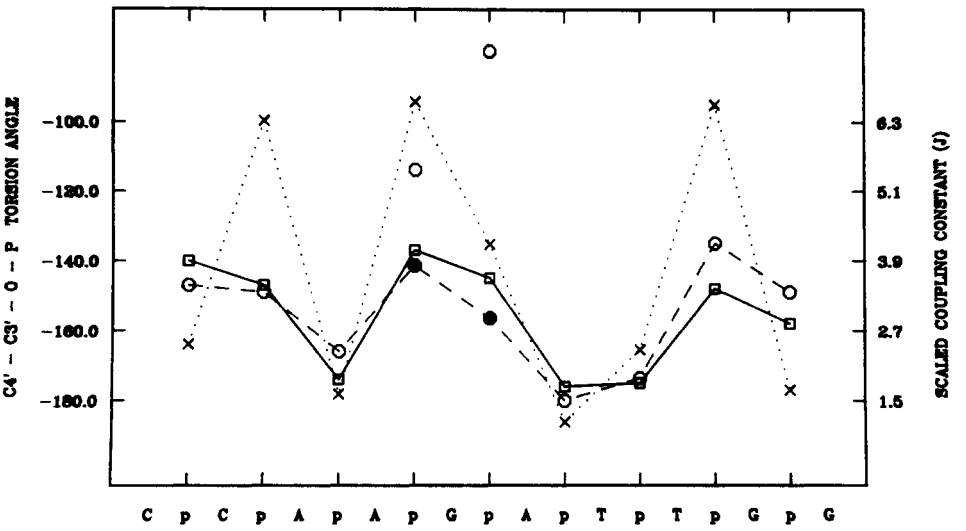

Figure 15. Plot of the ϵ torsion angle from the crystal structure (···×···) and final solution structure (–□–) vs phosphate position along the 5′–3′ strand for duplex decamer d(CCAAGATTGG)$_2$. The experimental $J_{H3'-P}$ coupling constant (--○--; --●--) vs phosphate position is also shown. The $J_{H3'-P}$ coupling constant vs sequence plot has been scaled to reflect the ϵ torsion angle variations. (Reprinted from ref 189. Copyright 1990 American Chemical Society.)

seem obvious that the mismatch will affect the chemical shift, it appears to do so in no predictable fashion. It was expected that a downfield chemical shift perturbation would be observed for the G5p and A6p resonances; however, this has proved to be only partially correct. Although the phosphorus resonance of the phosphate attached to the 3′-oxygen of G5 is shifted downfield, the phosphorus resonances 3′ to the mismatched A6 is not. Rather it is the phosphorus resonance attached to the 3′-oxygen of A4. Thus the backbone distortions of both mismatched base pair are evidenced on the 5′ side of the mismatched bases, pG5 and pA6.

The downfield shift of a single phosphorus resonance has been observed in other distorted duplex sequences as well. The extrahelical adenosine containing duplexes d(CGCGAAATTTACp*GCG)$_2$ and d(CCGGAATTCACp*GG)$_2$ previously studied[187,188] both contained a downfield-shifted phosphorus peak associated with the phosphate one residue removed to the 3′ side of the extrahelical base. The extrahelical cytosine-containing duplex d(CCGp*CGAATTCCGG)$_2$ also studied by Kalnik et al.[187] contains no anomalously downfield shifted ^{31}P peak; however, the phosphate attached to the 5′-oxygen of the extrahelical cytosine shifts downfield upon warming. This is unusual since warming has been observed to produce the opposite effect (i.e., an upfield movement of the affected ^{31}P resonance) for the phosphate at the site of an extrahelical adenosine duplex.[184] Additionally, the ^{31}P assignments of several sequences containing nonstandard base pairs have been determined in Gorenstein's laboratory.[118] These mismatches have been derived from the parent self-complementary dodecamer d(CGX$_1$GAATTCX$_2$CG)$_2$. In the A·G and C·A dodecamers (X$_1$·X$_2$) studied, it is the phosphorus attached to the 3′-oxygen of G2 which resonates downfield from the rest of the ^{31}P cluster. Contrarily, in the T·G and U·G mismatches, it is the phosphorus resonance of the phosphate on the 5′ side of the mismatched T and U (p11) which becomes the most downfield shifted peak. Finally, the G·G mismatch shows a downfield shift (although not as seen in the other sequences) of the T8p peak (one residue removed to the 5′ side of the mismatched G10 residue). It is thus clear that there appear to be no rules which would allow the prediction of where distortion relief might occur along the phosphate backbone (as monitored by ^{31}P NMR) in molecules such as those described above.

5. Comparison of the Phosphate Backbone Torsional Angle Variations from Solution Coupling Constants, NOESY Restrained Molecular Dynamics Calculations, and the X-ray Crystal Structure of the GA-Mismatch Decamer Duplex

As shown in Figure 15 the NOESY distance restrained MD calculations for the tandem GA-mismatch d(CCAAGATTGG)$_2$ are able to reproduce the observed variation in the ϵ torsional angles for the decamer as calculated from the experimental $J_{H3'-P}$ coupling constants.[189] (The ϵ torsional angles also rather accurately parallel the variation in ^{31}P chemical shifts; see ref 189.) The ϵ torsional angles were calculated by averaging over 160 ps dynamics of a 2D NOESY/hybrid matrix/restrained MD refinement. It is clear that a remarkably strong correlation exists between the pattern of the variation of the torsional angles derived from the restrained MD calculations and the experimentally measured coupling constants (the fit is poorer to an alternate conformation that is in slow chemical exchange; ○ in Figure 15). Similar correlations between the averaged torsional angles from restrained MD refinement of the d(CGCTTAAGCG)$_2$ base-paired B-DNA decamer have also been demonstrated.[21]

It is important to note that the ϵ torsional angles in Figure 15 derived from the restrained MD calculations represent time averages during which large amplitude fluctuations are observed on the picosecond time scale, similar to those shown in Figure 11. As found for the d(CGCTTAAGCG)$_2$ base-paired B-DNA decamer the time course of the restrained MD calculated fluctuations about the six sugar phosphate torsional angles in the GA-mismatch decamer show relatively small amplitude fluctuations about the average B-DNA values except for the ϵ and ζ torsional angles. These torsional angle

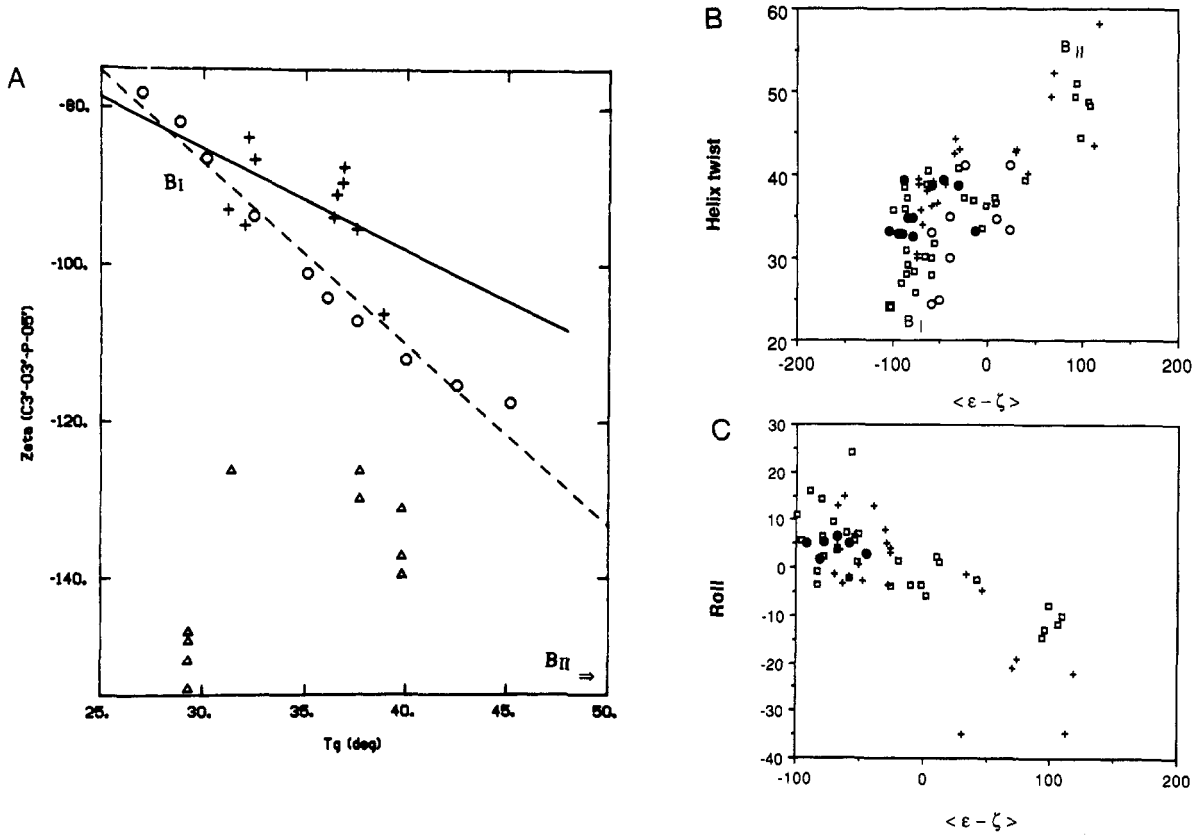

Figure 16. (A) Comparison of gas-phase calculations, solution conformational data, and X-ray crystallographic data on dodecamer d(CGCGAATTCGCG)$_2$. Plot of calculated ζ, P–O3′ torsional angles as a function of helix twist, t_g, based upon the AMBER, molecular mechanics energy-minimized dTpG·dCpA duplex dimer structures (--o--). Also shown are the ζ torsional angles derived from the X-ray crystal structures[27,28] of the dodecamer (– + –). The crystallographic data only includes B_I conformations and the residue at the ends of the duplex has been eliminated. Each conformation represents the average of phosphate conformations on complementary strands and has also been end-for-end averaged. The ζ torsional angles derived from the solution coupling constants[20,116] are also shown (△). Lines represent the best least-squares fit of the crystal and theoretical data. Part B shows a plot of helix twist (t_g) vs $\epsilon - \zeta$, and part C shows a plot of helix roll vs $\epsilon - \zeta$ (data from Hartmann et al.[122]): (□, +) based upon molecular dynamics simulations (+) and crystallographic studies (□). Experimentally derived structures for (CGCTTAAGCG)$_2$ (○) and d(TGTGAGCGCTCACA)$_2$ (●) duplexes from Gorenstein's laboratory. The latter results were calculated from 2D NOESY/restrained MD refinements ($\epsilon - \zeta$ were averaged over the MD refinement).[21,192] (Part A, reprinted from ref 20. Copyright 1988 American Chemical Society.)

changes again reflect a transition from the low-energy B_I conformation to the higher energy B_{II} conformation.

Figure 15 also demonstrates that the variation in the backbone conformation in the crystal state follows the same pattern of variation in the measured coupling constants and the averaged torsional angles derived from the restrained MD refinement. In the crystal state, most of the phosphates appear frozen in either pure B_I or pure B_{II} conformations. At any single snapshot of the restrained MD calculations, some phosphates are also frozen in pure B_I or pure B_{II} conformations (similar to that shown in Figure 11). However analysis of the ϵ torsional angle in any single snapshot during the MD trajectory leads to an incorrect value for the ϵ torsional angles as measured by the $J_{H3'-P}$ coupling constants. It is *only* the time average of the torsional angles that correctly describes the pattern of $J_{H3'-P}$ coupling constants. (In another tandem GA-mismatch duplex conformational constraints on the backbone are sufficiently strong so as to keep two of the phosphates locked in a B_{II} state—and the ^{31}P chemical shifts of these phosphates are shifted downfield as expected.[190] Similar downfield shifts in another GA-mismatch have been observed by Lane and co-workers.[191]) These results and those described in the previous section provide strong support for our hypothesis that *dynamic* variations in the backbone torsional angles are largely responsible for ^{31}P chemical shift variations in duplex oligonucleotides.

6. Correlation of Local Helical Geometry with Backbone Conformation

X-ray, NMR, and computational methods now all agree that there are major backbone conformational changes introduced as a result of sequence-specific, local helical variations. Dickerson and co-workers[27,28] had first noted that there appeared to be little correlation between the helical parameters and the deoxyribose phosphate backbone torsional angles in the crystal structures. A modeling study of an idealized Arnott B-DNA dinucleoside monophosphate duplex structures with sequence d(TG)·d(CA) in which the helix twist was varied from 25° to 45° while the helical height was kept fixed at 3.38° was carried out in Gorenstein's laboratory. The model-built structures were then energy refined.[20] The modeling results (Figure 16A, ○) showed that as the helix twist increases the phosphate ester conformation goes from a B_I to a B_{II}-type of conformation (i.e. ζ changes from g^- to t). Reanalysis of the crystallographically derived backbone torsional angles for the dodecamer d(CGCGAATTCGCG)$_2$ also showed a modest (Figure 16A, +)

correlation between t_g and ζ (R = −0.50) for the B_I phosphates[20] consistent with the model-calculated ζ torsional angle variations.[20] Significantly, the $D_{C4'C4'}$ distances obtained from the model duplex dimer and four crystal structures of the dodecamer duplex also followed a similar change as a function of t_g, similar to that shown in Figure 13.[20] While the calculated distances from the model-built dimer responded more steeply to the variation in t_g than the actual values, the trend was similar. This was reasonable since we were ignoring other helical adjustments (e.g., roll and base slide) which must also perturb the backbone length.

Hartmann et al.[122] have carried out another molecular modeling study of the relative energetics of the two phosphate ester conformations in the context of local helical structural variations. As shown in Figure 16, parts B and C, their very important results, comparing X-ray crystral structures and the modeling study,[20,122] provide additional strong support to the dependence of helical twist (and roll) on the backbone conformation (and of course indirectly on $J_{H3'-P}$ coupling constants and ^{31}P chemical shifts).[7,12,20,159] Recall that an ϵ–ζ value of −90° is associated with a B_I phosphate whereas a value of +90° is associated with a B_{II} phosphate. Included in this plot (as derived from ref 122) are values of 2D NOESY restrained MD calculated values of several tetradecamer and decamer duplexes calculated in my laboratory.[21,192] Especially for helix twist, the solution conformation generally follows the same variation observed in the crystal structures.

Clearly B_{II} phosphates are associated with high values of helix twist[20] and large negative values of helix roll.[119,122] High twist and low positive roll perturb the phosphate ester backbone and decrease base-stacking interactions in TpA relative to ApT.[119,193] Similar effects are noted for the Py–Pu sequence CpG vs Pu–Py sequence GpC.[119,193,194] As pointed out in ref 122 when both B_{II} phosphates are opposite each other in a duplex step, as the phosphates turn toward the minor groove, they force the base pairs to be displaced into the major groove by up to 2 Å. This results in some loss of stacking energy. With a large negative roll, the effect is to produce a kink toward the minor groove in the DNA at this juncture, producing a significant local bend in the duplex. Indeed in several instances of a GA mismatch, a very high twist value is found at a base step with either phosphates always in a B_{II} conformation[190] or with phosphates predominantly in the B_{II} conformation.[125] As indicated earlier, previous efforts to relate local helical parameters (as calculated from the Calladine rules) with ^{31}P spectral data led to marginal or poor correlations. There is however a much better correlation between *solution calculated values of helix twist* and phosphate conformation (and between ^{31}P chemical shifts and phosphate conformation) in DNA fragments.

Calculations have suggested that the energy barriers for a B_I/B_{II} transition vary between 4.6 and 15.0 kcal/mol with energy differences between the two states of 1.9–10.0 kcal/mol.[122] In one instance with symmetrically disposed B_{II} phosphates on both strands of the base step, the B_{II} phosphate was 3.6 kcal/mol lower energy than the B_I state. These results are consistent with the transitions that can be seen in the molecular dynamics trajectories of various base steps such as that shown in Figure 12. Similar transitions have been noted in MD studies in water with added counterions.[195,196]

Low-field phosphates generally appear to be associated with Py–Pu base steps[20,118,119,122,158] that have high helical twist. This produces an increase in the length of the sugar phosphate tether, lowering the relative energy difference (and energy barrier?) between the two phosphate states. This will produce a more flexible phosphate site in which transitions can occur more readily and in higher frequency, as appears to be observed in the MD simulations. As shown by El antri et al.[119] in a study of six related octamers, the four different base steps have the following average values: Pu–Py (AC, AT, GC, GT) −4.30 ppm ≥ Py–Py (TT, CT, TC) −4.28 > Pu–Pu (AA, AG, GA) −4.17 > Py–Pu (CA, CG, TA, TG) −4.08. These trends generally also appear in longer duplexes (generally with a wider chemical shift).[20,118,158] A strong correlation was also observed between observed $J_{H3'-P}$ coupling constant and ^{31}P chemical shifts in the octamers, again consistent with longer duplexes. El antri et al.[119] also note the strong correlation of helix twist with phosphate ester conformation and ^{31}P spectra. A CpG step shows low-field signals with large three-bond coupling constants while ApT show high-field signals with small three-bond coupling constants. Again as nicely noted by El antri et al.[119] in NOESY distance-restrained molecular dynamics calculations, the ApT Pu–Py step is ca. 30° in CApTG and the CpG Py–Pu step is 43° in ACpGT.[194,197]

As shown by the very similar ^{31}P chemical shifts, coupling constants and NMR calculated values of helix twist for various decamers and tetradecamers[20,118,158,192] the effects of sequence are largely localized at the base step *and* its one or two flanking nearest neighbors. Note in Figure 17, how the values of helix twist and roll between the two tetradecamers in regions outside of the G–C to A–T mutation (nts 4–10) are quite similar. In contrast, at the mutation site or adjacent to it there are large changes in helix twist (a 4–6° increase at positions 2, 3, 11, and 12) and roll (from +2 to −5° at positions 2 and 12). After taking into account those structures that might be influenced by crystal packing interactions, similar localization of the helical parameters is often noted for similar units of 4–6 base pairs. Indeed the original Calladine rules were based upon the idea that base step and the single nearest neighbor on either side defined local helical changes. It is quite likely that the failure of the simple Calladine rules arise from the neglect of another important variable in allowing DNA local geometry to respond to sequence: the conformation of the sugar phosphate backbone.

9. *lac* Repressor Headpiece–Operator ^{31}P NMR Spectra

How do proteins recognize DNA? Most attention on understanding the binding specificity between amino acid sequences and DNA sequences has centered on hydrogen bonding to the acceptor/donor groups on the Watson–Crick base pairs in the major groove (cf. ref 36). At present we do not understand this "second genetic code" of protein–DNA recognition. Perhaps one reason for the inability to dissect the basis for this specificity is the emphasis on base-pair interactions alone. In every high-resolution X-ray crystal structure

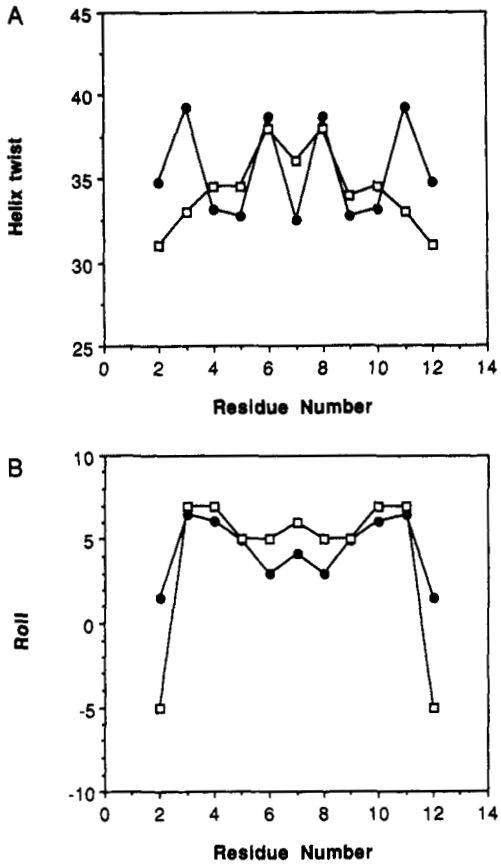

Figure 17. Plot of calculated helical twist (A) and roll (B) vs sequence for d(TGTGAGCGCTCACA)$_2$ (●) and G to A mutant d(TATGAGCGCTCATA)$_2$ (□).[192] Helicoidals calculated from 2D NOESY/restrained MD refinement methodology.

of a protein–DNA complex, the majority of the contacts are to the phosphates.[39-43] Perhaps localized, sequence-specific conformational variations in DNA which alter the position, conformation, and dynamics of the phosphate are another important component of a protein's recognition of specific sites on the DNA.[198,199]

The regulation of the expression of the *lac* genes has served as the archetypal example of a negatively controlled operon in prokaryotes.[200] While site-specific mutagenesis and mutant operators have proven to provide important information on the role of individual amino acids and base pairs in the recognition process[201,202] it is still not understood at a detailed molecular level.[203,204] X-ray crystallographic structural refinements, extensive mutagenesis experiments,[205-212] as well as model-building suggest that certain side-chain residues recognize the individual bases of nucleic acids, while others "recognize" the backbone phosphates, possibly through sequence-specific variations in the DNA conformation.

It is possible to duplicate the basic *lac* operator–*lac* repressor protein interaction by using the smaller *lac* repressor headpiece N-terminal domain fragment.[213-217] Recent NMR-derived structures of repressor headpiece bound to *lac* operator DNA fragments have begun to provide details confirming the sequence-specific interactions of a recognition α-helix binding within the major groove of the operator DNA. In this section, the ^{31}P NMR spectra of various 14-base pair *lac* operators free and bound to both wild-type and a Y7I (tyrosine 7 to isoleucine) mutant *lac* repressor headpiece proteins

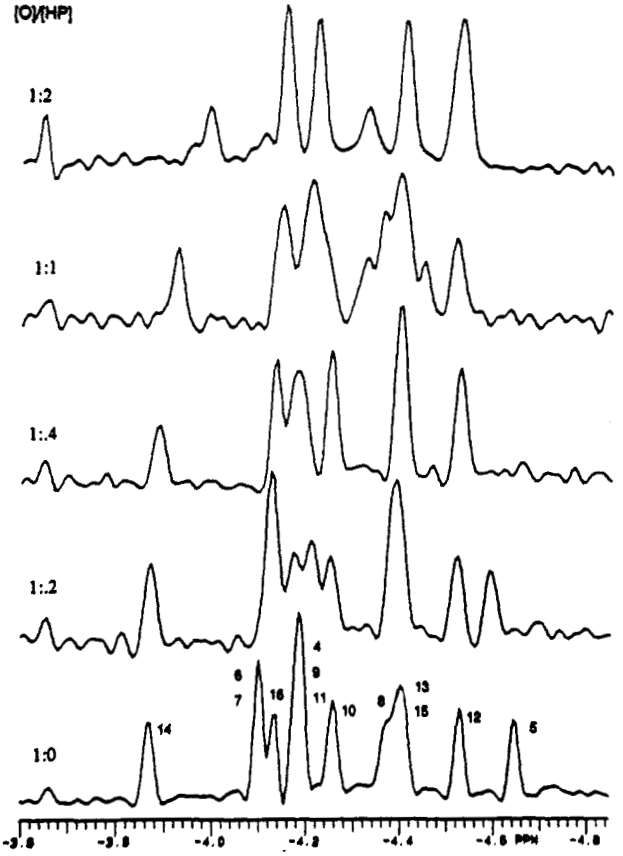

Figure 18. ^{31}P NMR spectra of the 14-bp oligonucleotide duplex, d(T*A*TGAGCGCTCA*TA*)$_2$ (mutant operator O2) as a function of the relative ratio of [14-bp operator]/[wild-type *lac* repressor headpiece] at ionic strength, 0.067 M. The [O]/[HP] ratios during the titration are shown. Numbering corresponds to phosphate position from the 5′-end of the duplexes, starting at position 4. (Reprinted from ref 199. Copyright 1992 American Chemical Society.)

are shown to provide information on the backbone conformation and dynamics in the complexes.

As illustrated in Figure 4, 2D pure absorption-phase constant time (PAC) heteronuclear correlation NMR[94,97] and ^{17}O–^{18}O labeling methodologies[7] have been used to assign the ^{31}P spectra of palindromic, wild-type *lac* operator 14-mer d(TGTGAGCGCTCACA)$_2$ (O1) as well as a number of base-pair mutants, d(T*A*TGAGCGCTCA*TA*)$_2$ (O2) and d(TGTG*T*GCGC*A*CACA)$_2$ (O3; complementary sites of mutation in the palindromic operators are italicized). These symmetrical base sequences are about two-thirds the length of the 21 base-pair wild-type sequence, and the 14-mers are believed to contain most of the important recognition sites[218,219] for the *lac* repressor protein. Mutagenesis studies[220] have indicated that repressor protein still binds, although less tightly, to operators containing either a single-site G to A transition at position 5 (O2) or an A to T transversion at position 8 (O3).

The ^{31}P spectral changes upon binding the N-terminal 56-residue headpiece (HP) to the 14-mer operators demonstrate that all of the phosphate resonances remain in fast chemical exchange during the entire course of the titration because only one set of peaks is observed at all DNA–protein ratios.[198] An example of the ^{31}P NMR spectra at various [O]/[HP] ratios for the mutant operator (O2) and wild-type headpiece is shown in Figure 18. At low ionic strength the ^{31}P

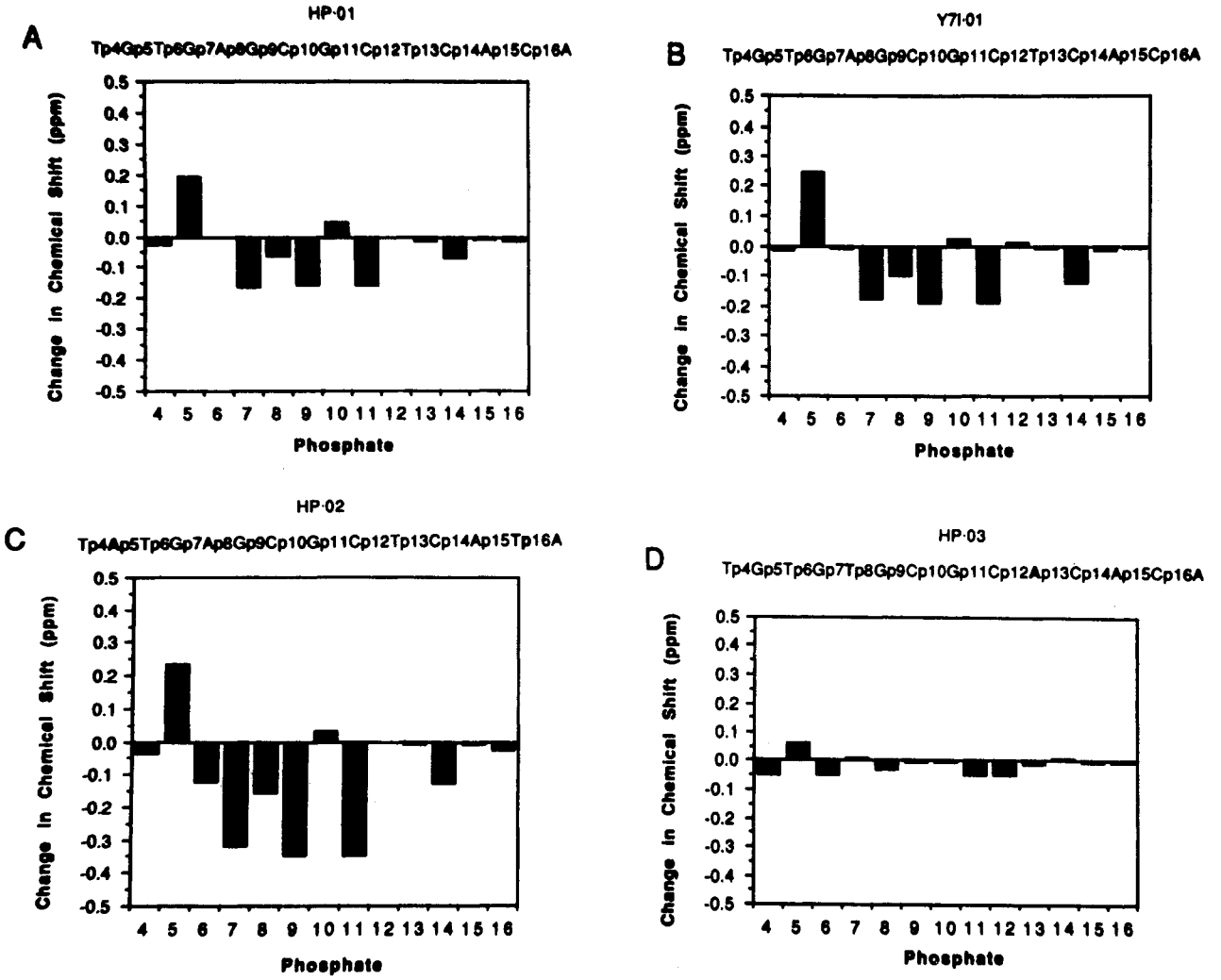

Figure 19. Summary bar plots of the perturbation of the ^{31}P chemical shift of individual phosphates of the 14-mer operators upon binding 2 equiv of the 56 residue *lac* repressor headpiece: (A) symmetric "wild-type" operator O1 and wild-type headpiece, (B) wild-type operator O1 and Y7I mutant headpiece, (C) O2 mutant operator and wild-type headpiece, and (D) O3 mutant operator and wild-type headpiece. (Reprinted from ref 199. Copyright 1992 American Chemical Society.)

spectral changes for all of the complexes level off at a ratio of two headpiece molecules (HP) per one operator duplex (O). Therefore, one headpiece is bound at each half of the operator (presumably to the dTGTGA wild-type recognition sequence).

In the wild-type O1 operator binding to the wild-type headpiece,[198] the ^{31}P signals of phosphates 5, 7, and 8 are well resolved at the beginning of the titration and show significant perturbation upon addition of headpiece. (The G5 phosphate shifts 0.20 ppm downfield while the G7 phosphate shifts 0.16 ppm upfield during the titration.) The A8 phosphate shifts 0.13 ppm upfield during the titration. The ^{31}P signals of phosphates 6, 9, and 11 are coincident in the absence of repressor and in the 2:1 complex two of the three shift 0.15 ppm upfield during the titration. The ^{31}P signals of the remaining phosphates 4, 10, and 12–16 show either no or small perturbations (<0.1 ppm) upon titration with headpiece. Assuming that the magnitude of the ^{31}P shift reflects the degree of interaction of the phosphate with the headpiece we can conclude that phosphates 5–8 (and possibly 9) represent a major binding site for the headpiece. A bar plot representation of the ^{31}P chemical shift perturbations is shown in Figure 19A.

In all of the complexes the range of ^{31}P chemical shifts in the free operators narrows upon binding either wild-type or mutant headpiece as the most upfield signal shifts downfield and the furthest downfield signal moves upfield. This presumably reflects a change to a more uniform conformation (more B_I-like) for all of the phosphates in all of the operator headpiece complexes. Consistent with this interpretation note that in the O1, O2, and O3 operators phosphate 5 is shifted *downfield* upon binding to either wild-type or Y7I headpiece (in O1 and O2 complexes it is the only phosphate that is shifted significantly downfield). In each of the O1–O3 operators, phosphate 5 is also the most upfield signal.

The interaction of O2 mutant operator with wild-type headpiece as monitored by ^{31}P NMR spectroscopy is also very similar to that of wild-type headpiece and wild-type O1 operator. The phosphate sites of interaction for this interaction are the same as those sites observed for the wild-type–wild-type operator repressor interaction. However, one difference is that the magnitude of the change in chemical shifts is *greater* for the O2 interaction than for any others that have been studied so far (Figure 19C). This is really quite remarkable because the mutant O2 operator binds more weakly to both the wild-type and Y71 mutant head-

pieces. Thus the magnitude of the ^{31}P perturbations is *not* reflective of the tightness of the complex.

As previously observed for sequence-specific ^{31}P chemical shift effects in the free operators, the ^{31}P chemical shifts are largely perturbed only at the sites surrounding the mutation.[158] Phosphates that are more than two positions removed generally have identical ^{31}P shifts as the wild-type sequence. Thus in the free mutant O2 operator, the ^{31}P chemical shifts of only phosphates p14 and p15 (and to a lesser extent p6 and p7) differ significantly from operator O1 even though the G5 → A5 (and C16 → T16) mutations might be expected to perturb nearest-neighbor phosphates p4–p7 and p14–p16. This indicates that the conformational state of all of the phosphates in O2 are very similar to their counterparts in O1 with the exception of p6, p7, p15, and p16. However, as shown by the bar plots of Figure 19, parts A–D, the ^{31}P chemical shifts of p15 and p16 are little changed in any of the complexes suggesting that the protein makes little contact with these phosphates.

The pattern of changes in the ^{31}P chemical shifts of the wild-type symmetrical O1 operator upon binding Y7I mutant headpiece were strikingly similar to the changes observed for the wild-type headpiece–operator complex (Figure 19, parts A and B).[198,199] This might be expected since the Y7I mutant repressor protein binds a 322 bp DNA fragment containing the wild-type nonpalindromic operator with only a 3-fold poorer binding constant than the wild-type repressor protein. Similarly, the operators bind ca. 10-fold poorer to the Y7I mutant headpiece with K_D's ca. 4.5×10^{-7} M to 6.7×10^{-7} M to the wild-type headpiece.[221] 2D ^1H NMR studies show that the mutation significantly disrupts the overall structure and stability of the recognition helix of the headpiece (residues 17–25; see ref 222). In the mutant, loss of the Y7–Y17 aromatic sidechain interaction, proposed to exist in the wild-type 56-residue headpiece, presumably selectively destabilizes the helix. The presence of nearly all of the tertiary structure cross-peaks[25] in the mutant protein indicates that the overall folding has not been dramatically altered. A model for the wild-type–wild-type complex derived by NOESY distance-restrained molecular dynamics calculations[223,224] shows the basic orientation of the recognition helix in the major groove of the operator near the dTGTGA site.

Analysis of ^{31}P Chemical Shift Perturbations in Protein–DNA Complexes. The perturbations in ^{31}P chemical shifts in forming the O–HP complex can arise from several sources. Electrostatics and local shielding effects by the bound protein certainly can play a role.[19] However, as described earlier, the ratio of B_I/B_{II} phosphate ester conformations play a dominant role in the ^{31}P chemical shift differences in small DNA fragments.[118] Any set of hydrogen-bonding donors or positively charged groups could readily discriminate between these two conformations that differ significantly in the orientation of the phosphoryl group and hence the electrostatic potential. These sequence-specific variations in the conformation of the DNA sugar phosphate backbone thus can possibly explain the sequence-specific recognition of DNA, as mediated through direct contacts and electrostatic complementarity between the phosphates and the protein.

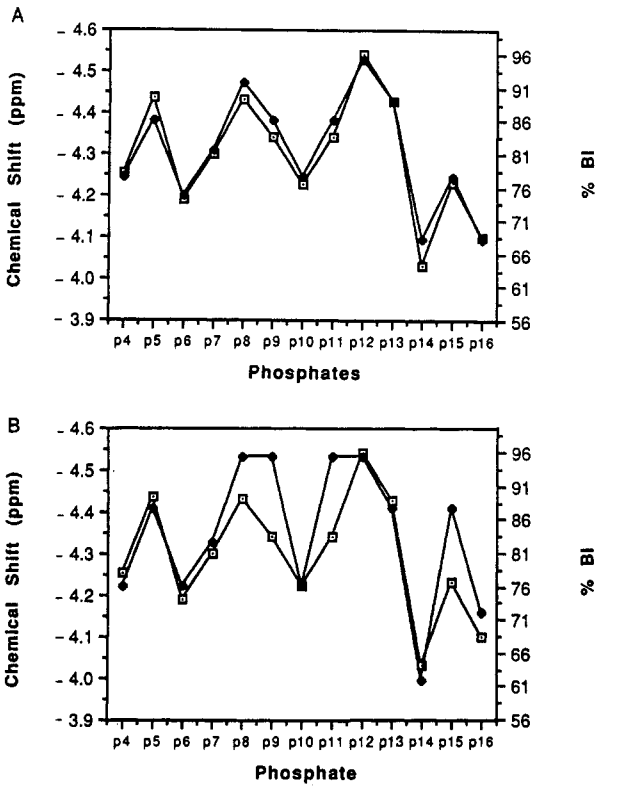

Figure 20. Plot of ^{31}P chemical shifts (◆) vs sequence for (A) wild-type O1 operator·Y7I mutant headpiece and (B) mutant O2 operator–wild-type headpiece. The ^{31}P chemical shifts (□) vs sequence for the wild-type O1 operator–wild-type headpiece is shown for comparison. The percentage of the B_I phosphate backbone conformation calculated from the ^{31}P chemical shifts as described previously is also shown. (Reprinted from ref 199. Copyright 1992 American Chemical Society.)

Assuming then that the ^{31}P chemical shifts also represent the relative populations of the B_I and B_{II} states in the HP–O complexes, then we can calculate the fractional populations by assuming a simple two-state model. A plot of ^{31}P chemical shifts (and B_I/B_{II}) populations vs sequence for several of the operator complexes is shown in Figure 20. Note as expected for the very similar perturbation in ^{31}P chemical shifts in the O1 wild type and Y7I mutant headpiece complexes, the pattern of sequence-specific variation in ^{31}P chemical shifts in the two complexes are very similar (Figure 20A). In the *lac* O2 mutant operator–headpiece complex several of the phosphates are significantly perturbed from the phosphate ester populations in the O1–HP complex. Phosphates such as p6, p8 and p11 in the O2 complex are apparently constrained to a B_I conformation (Figure 20B; p15 is also shifted to a more B_I-type state). Other complexes (including ones described in more detail in ref 221) have 2–4 phosphates constrained to a more B_I-like state. This is a reflection that almost all of the ^{31}P signals are shifted upfield (more B_I-like) as shown in the bar plots of Figure 19.

These results have suggested that discrimination between the operators may be based upon the degree to which the repressor protein restricts phosphate ester conformational freedom in the complex.[199,221] Specific, tightly bound complexes apparently *retain the inherent phosphate ester conformational flexibility of the operator itself*, whereas more weakly bound operator–protein complexes restrict the phosphate ester con-

formationally freedom in the complex relative to the free DNA. It is especially intriguing that alternating Py–Pu sequences show enhanced flexibility, not only in the sugar phosphate backbone[21,24] but in the overall conformation of the duplex.[120,225] The identical 5′-dTGTG·5′-dCACA recognition sequence in an O_R3 operator mutant of λ phage and in the complex with the sequence-specific DNA binding protein Cro shows unusual flexibility based upon gel circularization assays.[120] In contrast the averaged static structure appears to be quite normal. NMR structural studies[225–227] indicate a partial unstacking of bases in one strand in a GTG·CAC triplet. The high properties of B_{II} phosphates in the same 5′-dTGTG·5′-dCACA region of the *lac* operator also signify increased flexibility of this sequence. Interestingly the GTG·CAC sequence is often observed in gene regulatory regions.[120,225,228]

This proposal based upon the loss of conformational freedom in the complex contributing to specificity of interaction can also explain the 10-fold reduction in binding of Y7I mutant to wild-type operator. The first two helices of the Y7I mutant headpiece are partially disordered,[222] which is not the case for wild-type headpiece. In order for the second, recognition helix to bind within the major groove of the operator, this disorder or dynamic flexibility must be removed. Conformational restriction of the peptide backbone will be entropically unfavorable, presumably reflected in the weaker association of the mutant headpiece. (In wild-type headpiece, the recognition helix is already conformationally restricted and no entropy must be lost in order for it to fold and bind to operator).

Thus these studies suggest that optimal protein–DNA recognition will require a balance between the dynamics of both the protein and DNA. Too rigid of a protein will lock up the phosphates, reducing affinity. If the protein is too flexible then a certain amount of entropy will be lost as the secondary structure is ordered to allow operator binding and recognition. This requirement for *retention* of DNA and protein backbone torsional freedom in strongly bound complexes (which is entropically favorable) provides a new mechanism for protein discrimination of different operator binding sites. Thus upon binding, various rotational degrees of freedom must be lost if the repressor were to bind to only one of the phosphate conformations. The dissociation constant will reflect this internal entropic disadvantage, which may be as large as 8 eu (2.4 kcal/mol at 25 °C) per lost degree of torsional freedom.[229] For freezing two rotational degrees of freedom, this entropic factor may represent a binding difference of up to 10^3–10^4. In duplex DNA, of course, the phosphodiester bonds of the different phosphates are already partially conformationally constrained and the entropic penalty will be much less (however, at least a factor of RT ln 2 or ca. 0.4 kcal/mol at room temperature). As described in the previous sections, X-ray crystal structures, solution NMR structures, and molecular dynamics simulations demonstrate that the most conformationally mobile portion of the DNA is the phosphate ester.[19] Binding of the repressor in such a way as to restrict the intrinsic conformational freedom of 10 or more of the operator phosphates could, in principle, contribute to a sizable entropic disadvantage.

This analysis suggests another explanation both for the entropy differences in the binding of various wild-type and specific mutant operator for repressor as well an entirely new appreciation for the difficulty in which a protein must recognize the structural features *and dynamics* of operator DNA. Thus in the strongly bound, specific complexes the protein must not only provide a binding surface that matches the sequence-specific variation in the phosphate conformation of the operator but also allow for retention of the phosphate conformational freedom in the complex. The position of the phosphate will move in changing from a B_I to a B_{II} state and indeed the position of the phosphate shows the greatest RMS variation in molecular dynamics calculations.[230] This will place enormous constraints on the protein structure in the complex if the phosphate ester conformational freedom is not to be greatly reduced in the complex. This can only be possible if the protein–DNA interface is flexible enough and if there is a "coupling" of the motion of the amino acid residues in the binding site with the phosphate ester motion. In contrast in a specific mutant operator that does not bind as strongly to the repressor, the subtle structural and dynamical requirements for providing the necessary coupling or flexibility is presumably lost so as to preclude free torsion of at least some of the phosphate esters in the protein–DNA complex. Recall that in the wild-type O1-wild-type HP complex the ^{31}P data suggests that only one of the phosphate appears to be restricted to a B_I state. In contrast, in all of the mutant complexes (operators and/or headpiece) 2–4 phosphates are "frozen" in a B_I conformational state.

Therefore a significant requirement for an "evolutionarily perfected" repressor to strongly bind a specific operator is to allow sufficient flexibility in the complex such that the phosphate can still jump between the B_I and B_{II} states.[199] It should not be so flexible that in its free state the recognition helix is disordered. In mutant operators and proteins presumably the structural and dynamical coupling between the protein and DNA is disrupted such that the DNA and/or the protein backbone conformational freedom in the complex is greatly restricted through either steric or electrostatic interactions.

10. Conclusions

Through multidimensional heteronuclear NMR or ^{17}O labeling experiments it is now possible to unambiguously assign the ^{31}P signals of modest-sized duplex oligonucleotides. J(H3′–P) coupling constants (and hence the ε (C4′–C3′–O3′–P) torsional angles) can now also be measured. Correlations between experimentally measured coupling constants (and thus to P–O and C–O torsional angles) show that sequence-specific variations in ^{31}P chemical shifts are attributable to sequence-specific changes in the deoxyribose phosphate backbone. By analysis of the multiplet patterns in ^1H–^{13}C natural abundance HMQC and HSQC spectra, it is now also possible to extract additional carbon and proton coupling constants to phosphorus. There is little question that ^{31}P chemical shifts, ^{31}P–^1H and ^{31}P–^{13}C coupling constants will serve as an important probe of the conformation and dynamics of nucleic acids, particularly the deoxyribose phosphate backbone.

Acknowledgments. Supported by NIH (AI27744), the Purdue University Biochemical Magnetic Resonance Laboratory which is supported by the NSF-designated Biological Facilities Center on Biomolecular NMR, Structure and Design at Purdue (grants BBS 8614177 and DIR-9000360 from the Division of Biological Instrumentation) and the NIH-designated AIDS Research Center at Purdue (AI727713). The contributions of Christine Karslake, Maria Victoria Botuyan, David Keire, Indrasiri Kumaralal, Edward Nikonowicz, Vikram A. Roongta, Robert Powers, Claude R. Jones, Dean Carlson, Josepha Fu, Stephen A. Schroeder, James T. Metz, Robert Powers, Bruce Luxon, Robert Meadows, Carol Post, and Robert Santini are much appreciated.

References

(1) Gorenstein, D. G. *Phosphorus-31 NMR: Principles and Applications*; Gorenstein, D. G., Ed.; Academic Press: Orlando, 1984; pp 1–604.
(2) Gait, M. J. *Oligonucleotide Synthesis: a Practical Approach*; IRL Press: Oxford, 1984.
(3) Scaringe, S. A.; Francklyn, C.; Usman, N. *Nucleic Acids Res.* **1990**, *18*, 5433–5441.
(4) Feigon, J.; Leupin, W.; Denny, W. A.; Kearns, D. R. *Biochemistry* **1983**, *22*, 5943–5951.
(5) Feigon, J.; Leupin, W.; Denny, W. A.; Kearns, D. R. *Biochemistry* **1983**, *22*, 5943–5951.
(6) Hare, D. R.; Wemmer, D. E.; Chou, S. H.; Drobny, G.; Reid, B. *J. Mol. Biol.* **1983**, *171*, 319.
(7) Schroeder, S. A.; Fu, J. M.; Jones, C. R.; Gorenstein, D. G. *Biochemistry* **1987**, *26*, 3812–3821.
(8) Kearns, D. R. *Crit. Rev. Biochem.* **1984**, *15*, 237–290.
(9) Frechet, D.; Cheng, D. M.; Kan, L. S.; Ts'O, P. O. P. *Biochemistry* **1983**, *22*, 5194–5200.
(10) Broido, M. A.; Zon, G.; James, T. L. *Biochem. Biophys. Res. Commun.* **1984**, *119*, 663–670.
(11) Scheek, R. M.; Boelens, R.; Russo, N.; van Boom, J. H.; Kaptein, R. *Biochemistry* **1984**, *23*, 1371–1376.
(12) Schroeder, S.; Jones, C.; Fu, J.; Gorenstein, D. G. *Bull. Magn. Reson.* **1986**, *8*, 137–146.
(13) Pardi, A.; Walker, R.; Rapoport, H.; Wider, G.; Wüthrich, *J. Am. Chem. Soc.* **1983**, *105*, 1652.
(14) Lai, K.; Shah, D. O.; Derose, E.; Gorenstein, D. G. *Biochem. Biophys. Res. Commun.* **1984**, *121*, 1021.
(15) Gorenstein, D. G. *Phosphorus-31 NMR: Principles and Applications*; Gorenstein, D. G., Ed.; Academic Press: Orlando, 1984; pp 7–36.
(16) Gorenstein, D. G. *Annu. Rev. Biophys. Bioengin.* **1981**, *10*, 355.
(17) Gorenstein, D. G.; Findlay, J. B.; Momii, R. K.; Luxon, B. A.; Kar, D. *Biochemistry* **1976**, *15*, 3796–3803.
(18) Gorenstein, D. G. *Chem. Rev.* **1987**, *87*, 1047–1077.
(19) Gorenstein, D. G. *DNA Structures, Methods in Enzymology*; Lilley, D. M., Dahlberg, J. E., Eds.; Academic Press, Inc.: Orlando, FL, 1992; pp 254–286.
(20) Gorenstein, D. G.; Schroeder, S. A.; Fu, J. M.; Metz, J. T.; Roongta, V. A.; Jones, C. R. *Biochemistry* **1988**, *27*, 7223–7237.
(21) Powers, R.; Jones, C. R.; Gorenstein, D. G. *J. Biomol. Struct. Dyn.* **1990**, *8*, 253–294.
(22) Sundaralingam, M. *Biopolymers* **1969**, *7*, 821–860.
(23) Powers, R.; Gorenstein, D. G. *Biochemistry* **1990**, *29*, 9994–10008.
(24) Nikonowicz, E. P.; Meadows, R. P.; Fagan, P.; Gorenstein, D. G. *Biochemistry* **1991**, *30*, 1323–1334.
(25) Wisniowski, P.; Karslake, C.; Piotto, M. E.; et al. *Structure & Function*; Sarma, R. H., Sarma, M. H., Eds.; Adenine Press: Schenectady, NY, 1992; pp 17–54.
(26) van de Ven, F. J. M.; Hilbers, C. W. *Eur. J. Biochem.* **1988**, *178*, 1–38.
(27) Dickerson, R. E. *J. Mol. Biol.* **1983**, *166*, 419–441.
(28) Dickerson, R. E.; Drew, H. R. *J. Mol. Biol.* **1981**, *149*, 761–786.
(29) Saenger, W. *Principles of Nucleic Acid Structure*; Springer-Verlag: New York, 1984.
(30) Kennard, O.; Hunter, W. N. *Angew. Chem., Int. Ed. Engl.* **1991**, *30*, 1254–1277.
(31) Rinkel, L. J.; van der Marel, G. A.; van Boom, J. H.; Altona, C. *Eur. J. Biochem.* **1987**, *163*, 275–286.
(32) Clore, G. M.; Gronenborn, A. M.; Brunger, A. T.; Karplus, M. *J. Mol. Biol.* **1985**, *186*, 435–455.
(33) Patel, D. J.; Kozlowski, S. A.; Bhatt, R. *Proc. Natl. Acad. Sci.* **1983**, *80*, 3908–3912.
(34) Assa-Munt, N.; Kearns, D. R. *Biochemistry* **1984**, *23*, 791.
(35) Patel, D. J.; Shapiro, L.; Hare, D. *Biophys. Chem.* **1987**, *16*, 423–454.
(36) Landschulz, W. H.; Johnson, P. F.; McKnight, S. L. *Science* **1988**, *240*, 1759–1764.
(37) Matthews, B. W. *Nature* **1988**, *335*, 294–295.
(38) Klug, A.; Viswamitra, M. A.; Kennard, O.; Shakked, Z.; Steitz, T. A. *J. Mol. Biol.* **1979**, *131*, 669–680.
(39) Wolberger, C.; Dong, Y.; Ptashne, M.; Harrison, S. C. *Nature* **1988**, *335*, 789–795.
(40) Jordan, S. R.; Pabo, C. O. *Science* **1988**, *242*, 893–899.
(41) Otwinowski, Z.; Schevitz, R. W.; Zhang, R. G.; Lawson, C. L.; Joachimiak, A.; Marmorstein, R. Q.; Luisi, B. F.; Sigler, P. B. *Nature* **1988**, *335*, 321.
(42) Beamer, L. J.; Pabo, C. O. *J. Mol. Biol.* **1992**, *227*, 177–196.
(43) Somers, W. S.; Phillips, S. E. V. *Nature* **1992**, *359*, 387–393.
(44) Pavletich, N. P.; Pabo, C. O. *Science* **1993**, *261*, 1701–1707.
(45) Staacke, D.; Walter, B.; Kisters-Woike, B.; Wilken-Bergmann, B.; Müller-Hill, B. *EMBO J.* **1990**, *9*, 1963–1967.
(46) Marmorstein, R. Q.; Sprinzl, M.; Sigler, P. B. *Biochemistry* **1991**, *30*, 1141–1148.
(47) Haran, T. E.; Joachimiak, A.; Sigler, P. B. *EMBO J.* **1992**, *11*, 3021–3030.
(48) Schultz, S. C.; Shields, G. C.; Steitz, T. A. *Science* **1991**, *253*, 1001–1007.
(49) Chen, C. W.; Cohen, J. S. *Phosphorus-31: NMR Principles and Applications*; Gorenstein, D. G., Ed.; Academic Press, Inc.: Orlando, 1984; pp 233–263.
(50) Gorenstein, D. G.; Meadows, R. P.; Metz, J. T.; Nikonowicz, E. P.; Post, C. B. *Advances in Biophysical Chemistry*; Bush, C. A., Ed.; JAI Press: Greenwich, 1990; pp 47–124.
(51) Gorenstein, D. G.; Goldfield, E. M. *Phosphorus-31 NMR: Principles and Applications*; Gorenstein, D. G., Ed.; Academic Press: Orlando, 1984; pp 299–316.
(52) Tsai, M. D. *Phosphorus-31 NMR: Principles and Applications*; Gorenstein, D. G., Ed.; Academic Press: Orlando, 1984; pp 175–197.
(53) Hart, P. A. *Phosphorus-31 NMR: Principles and Applications*; Gorenstein, D. G., Ed.; Academic Press: Orlando, 1984; pp 317–347.
(54) James, T. L. *Phosphorus-31 NMR: Principles and Applications*; Gorenstein, D. G., Ed.; Academic Press: Orlando, 1984; pp 349–400.
(55) Harris, R. K. *Nuclear Magnetic Resonance Spectroscopy*; Pitman Books: London, 1983; pp 1–250.
(56) Shindo, H. *Phosphorus-31 NMR: Principles and Applications*; Gorenstein, D. G., Ed.; Academic Press: Orlando, 1984.
(57) Herzfeld, J.; Griffin, R. G.; Haberkorn, R. A. *Biochemistry* **1978**, *17*, 2711.
(58) Kohler, S. J.; Klein, M. P. *Biochemistry* **1976**, *15*, 967.
(59) Tutunjian, P.; Tropp, J.; Waugh, J. *J. Am. Chem. Soc.* **1983**, *105*, 4848–4849.
(60) Cheetham, A. K.; Clayden, N. J.; Dobson, C. M.; Jakeman, R. J. B. *J. Chem. Soc. Chem. Commun.* **1986**, 195–197.
(61) Ye, H.; Fung, B. M. *J. Magn. Reson.* **1983**, *51*, 313–317.
(62) Letcher, J. H.; Van Wazer, J. R. *J. Chem. Phys.* **1966**, *44*, 815–529.
(63) Letcher, J. H.; Van Wazer, J. R. *Top. Phosphorus Chem.* **1967**, *5*, 75–266.
(64) Rajzmann, M.; Simon, J. C. *Org. Magn. Reson.* **1975**, *7*, 334–338.
(65) Wolff, R.; Radeglia, V. R. *Z. Phys. Chem. (Leipzig)* **1980**, *261*, 726–744.
(66) Weller, T.; Deininger, D.; Lochman, R. *Z. Chem.* **1981**, *21*, 105–106.
(67) Bernard-Moulin, P.; Pouzard, G. *J. Chim. Phys.* **1979**, *76*, 708–713.
(68) Chestnut, D. B. *Phosphorus-31 NMR Spectroscopy in Stereochemical Analysis: Organic Compounds and Metal Complexes*; Verkade, J. G., Quin, L. D., Eds.; VCH Publishers: Deerfield Beach, FL, 1987; pp 185–204.
(69) Prado, F. R.; Geissner-Prettre, C.; Pullman, B.; Daudey, J. P. *J. Am. Chem. Soc.* **1979**, *101*, 1737–1742.
(70) Giessner-Pettre, C.; Pullman, B.; Prado, F. R.; Cheng, D. M.; Ivorno, V.; Ts'o, P. O. *Biopolymers* **1984**, *23*, 377–388.
(71) Gorenstein, D. G. *J. Am. Chem. Soc.* **1975**, *97*, 898–900.
(72) Purdela, D. *J. Magn. Reson.* **1971**, *5*, 23–26.
(73) Kumamoto, J.; Cox, J. R., Jr.; Westheimer, F. H. *J. Am. Chem. Soc.* **1956**, *78*, 4858–4860.
(74) Blackburn, G. M.; Cohen, J. S.; Weatherall, I. *Tetrahedron* **1971**, *27*, 2903–2912.
(75) Martin, J.; Robert, J. B. *Org. Magn. Reson.* **1981**, *15*, 87–93.
(76) Contractor, S. R.; Hursthouse, M. B.; Shaw, L. S.; Shaw, R. A.; Yilmaz, H. Personal communication.
(77) Dutasta, J. P.; Robert, J. B.; Wiesenfeld, L. *Phosphorus Chemistry*; Quin, L. D., Verkade, J. G., Eds.; American Chemical Society: Washington, D.C., 1981; pp 581–584.
(78) Smith, K. A.; Kirkpatrick, R. J.; Oldfield, E.; Henderson, D. M. *Am. Mineral.* **1983**, *68*, 1206.
(79) Gorenstein, D. G.; Kar, D. *Biochem. Biophys. Res. Commun.* **1975**, *65*, 1073–1080.
(80) Gorenstein, D. G. *Prog. Nucl. Magn. Reson. Spectroscop.* **1983**, *161*, 1–98.
(81) Prive, G. G.; Heinemann, U.; Chandrasegaran, S.; Kan, L.; Kopka, M. L.; Dickerson, R. E. *Science* **1987**, *238*, 498–504.
(82) Gupta, G.; Bansal, M.; Sasisekharan, V. *Proc. Natl. Acad. Sci. U.S.A.* **1980**, *77*, 6486–6490.

(83) Jain, S.; Sundaralingam, M. *J. Biol. Chem.* **1989**, *264*, 12780–12784.
(84) Dickerson, R. E.; Goodsell, D. S.; Kopka, M. L.; Pjura, P. E. *J. Biomol. Struct. Dyn.* **1987**, *5*, 557–579.
(85) Heinemann, U.; Alings, C. *EMBO J.* **1991**, *10*, 35–43.
(86) Lerner, D. B.; Kearns, D. R. *J. Am. Chem. Soc.* **1980**, *102*, 7612–7613.
(87) Costello, A. J. R.; Glonek, T.; Van Wazer, J. R. *J. Inorg. Chem. Soc.* **1976**, *15*, 972–974.
(88) Gorenstein, D. G.; Goldfield, E. M.; Chen, R.; Kovar, K.; Luxon, B. A. *Biochemistry* **1981**, *20*, 2141–2150.
(89) Gorenstein, D. G. *Jerusalem Symposium, NMR in Molecular Biology*; Pullman, B., Ed.; D. Reidel Publishing Co.: 1978; pp 1–15.
(90) Gorenstein, D. G.; Karslake, C.; Granger, J. N.; Cho, Y.; Piotto, M. E. *Phosphorus Chemistry*; Walsh, E. N., Griffith, E. J., Parry, R. W., Quin, L. D., Eds.; ACS Symposium Series; American Chemical Society: Washington, DC, 1992; pp 202–217.
(91) Petersheim, M.; Mehdi, S.; Gerlt, J. A. *J. Am. Chem. Soc.* **1984**, *106*, 439–440.
(92) Connolly, B. A.; Eckstein, F. *Biochemistry* **1984**, *23*, 5523–5527.
(93) Shah, D. O.; Lai, K.; Gorenstein, D. G. *J. Am. Chem. Soc.* **1984**, *106*, 4302.
(94) Fu, J. M.; Schroeder, S. A.; Jones, C. R.; Santini, R.; Gorenstein, D. G. *J. Magn. Reson.* **1988**, *77*, 577–582.
(95) Joseph, A. P.; Bolton, P. H. *J. Am. Chem. Soc.* **1984**, *106*, 437–439.
(96) Cheng, D. M.; Kan, L. S.; Miller, P. S.; Leutzinger, E. E.; Ts'O, P. O. P. *Biopolymers* **1982**, *21*, 697–701.
(97) Sklenár, V.; Miyashiro, H.; Zon, G.; Miles, H. T.; Bax, A. *FEBS Lett.* **1986**, *208*, 94–98.
(98) Jones, C. R.; Schroeder, S. A.; Gorenstein, D. C. *J. Magn. Reson.* **1988**, *80*, 370–374.
(99) Zagorski, M. G.; Norman, D. G. *J. Magn. Reson.* **1989**, *83*, 167–172.
(100) Bearden, D. W.; Brown, L. R. *Chem. Phys. Lett.* **1989**, *163*, 432–436.
(101) Morris, G. A.; Gibbs, A. *J. Magn. Reson.* **1991**, *91*, 444–449.
(102) Artemov, D. Y. *J. Magn. Reson.* **1991**, *91*, 405–407.
(103) Kellogg, G. W. *J. Magn. Reson.* **1992**, *98*, 176–182.
(104) Kellogg, G. W.; Szewczak, A. A.; Moore, P. B. *J. Am. Chem. Soc.* **1992**, *114*, 2727–2728.
(105) Hiroaki, H.; Uesugi, S. *FEBS Lett.* **1989**, *244*, 43–46.
(106) Williamson, D.; Bax, A. *J. Magn. Reson.* **1988**, *76*, 174–177.
(107) Chary, K. V. R.; Rastogi, V. K.; Govil, G. *J. Magn. Reson.* **1993**, *102*, 81–83.
(108) Kellogg, G. W.; Schweitzer, B. I. *J. Biomol.* **1993**, *3*, 577–595.
(109) Nikonowicz, E. P.; Pardi, A. *J. Am. Chem. Soc.* **1992**, *114*, 1082–1083.
(110) Nikonowicz, E. P.; Pardi, A. *Nature* **1992**, *355*, 184–186.
(111) Pardi, A.; Nikonowicz, E. P. *J. Am. Chem. Soc.* **1992**, *114*, 9202–9203.
(112) Kessler, H.; Griesinger, C.; Zarbock, J.; Loosli, H. R. *J. Magn. Reson.* **1984**, *57*, 331–336.
(113) Scheek, R. M.; Boelens, R.; Russo, N.; van Boom, J. H.; Kaptein, R. *Biochemistry* **1984**, *23*, 1371–1376.
(114) Frey, M. H.; Leupin, W.; Sørensen, O. W.; Denney, W. A.; Ernst, R. R.; Wüthrich, *Biopolymers* **1985**, *24*, 2371–2380.
(115) Schmieder, P.; Ippel, J. H.; Vandenelst, H.; van der Marel, G. A.; van Boom, J. H.; Altona, C.; Kessler, H. *Nucleic Acids Res.* **1992**, *20*, 4747–4751.
(116) Sklenar, V.; Bax, A. *J. Am. Chem. Soc.* **1987**, *109*, 7525–7526.
(117) Ragg, E.; Mondelli, R.; Garbesi, A.; Colonna, F. P.; Battistini, C.; Vioglio, S. *Magn. Reson. Chem.* **1989**, *27*, 640–646.
(118) Roongta, V. A.; Jones, C. R.; Gorenstein, D. G. *Biochemistry* **1990**, *29*, 5245–5258.
(119) El antri, S.; Bittoun, P.; Mauffret, O.; Monnot, M.; Convert, O.; Lescot, E.; Fermandjian, S. *Biochemistry* **1993**, *32*, 7079–7088.
(120) Lyubchenko, Y. L.; Shlyakhtenko, L. S.; Appella, E.; Harrington, R. E. *Biochemistry* **1993**, *32*, 4121–4127.
(121) Lankhorst, P. P.; Haasnoot, C. A. G.; Erkelens, C.; Altona, C. *J. Biomol. Struct. Dynam.* **1984**, *1*, 1387–1405.
(122) Hartmann, B.; Piazzola, D.; Lavery, R. *Nucleic Acids Res.* **1993**, *21*, 561–568.
(123) Shakked, Z.; Rabinovitch, D. *Prog. Biophys. Molec. Biol.* **1986**, *47*, 159–195.
(124) Chou, S. H.; Cheng, J. W.; Reid, B. R. *J. Mol. Biol.* **1992**, *228*, 138–155.
(125) Nikonowicz, E. P.; Gorenstein, D. G. *Biochemistry* **1990**, *29*, 8845–8858.
(126) Patel, D. J. *Biochemistry* **1974**, *13*, 2388–2395.
(127) Schwalbe, H.; Samstag, W.; Engels, J. W.; Bermel, W.; Griesinger, C. *J. Biomol. NMR* **1993**, *3*, 479–486.
(128) Gorenstein, D. G. *Methods in Enzymology*; James, T. L., Oppenheimer, N., Eds.; Academic Press, Inc.: San Diego, CA, 1989; pp 295–316.
(129) Un, S.; Klein, M. P. *J. Am. Chem. Soc.* **1989**, *111*, 5119–5124.
(130) Gueron, M.; Shulman, R. G. *Proc. Natl. Acad. Sci. U.S.A.* **1975**, *72*, 3482–3485.
(131) Gorenstein, D. G.; Goldfield, E. M. *Mol. Cell. Biochem.* **1982**, *46*, 97.
(132) Gorenstein, D. G.; Luxon, B. A.; Findlay, J. B. *Biochem. Biophys. Acta* **1977**, *475*, 184–190.
(133) Searle, M. S.; Lane, A. N. *FEBS Lett.* **1992**, *297*, 292–296.
(134) Forster, M. J.; Lane, A. N. *Eur. Biophys. J.* **1990**, *18*, 347–355.
(135) Alderfer, J. L.; Hazel, G. L. *J. Am. Chem. Soc.* **1981**, *103*, 5925–5926.
(136) Shindo, H.; Simpson, R. T.; Cohen, J. S. *J. Biol. Chem.* **1979**, *254*, 8125–8128.
(137) Eckstein, F.; Jovin, T. M. *Biochemistry* **1983**, *22*, 4546–4550.
(138) Chen, C. W.; Cohen, J. S.; Behe, M. *Biochemistry* **1983**, *22*, 2136–2142.
(139) Patel, D. J.; Canuel, L. L.; Pohl, F. M. *Proc. Natl. Acad. Sci. U.S.A.* **1979**, *76*, 2508–2511.
(140) Cohen, J. S.; Wooten, J. B.; Chatterjee, C. L. *Biochemistry* **1981**, *20*, 3049–3055.
(141) Hall, K.; Cruz, P.; Tinoco, I., Jr.; Jovin, T. M.; van de Sande, J. H. *Nature* **1984**, *311*, 584–586.
(142) Gorenstein, D. G.; Luxon, B. A.; Goldfield, E.; Lai, K.; Vegeais, D. *Biochemistry* **1982**, *21*, 580–589.
(143) Rich, A.; Nordheim, A.; Wang, A. H. J. *Ann. Rev. Biochem.* **1984**, *53*, 791–846.
(144) Drew, H.; Takano, T.; Tanaka, S.; Itakura, K.; Dickerson, R. E. *Nature* **1980**, *286*, 567–573.
(145) Brennan, R. G.; Westhof, E.; Sundaralingam, M. *J. Biomol. Struct. Dyn.* **1986**, *3*, 649–663.
(146) Sklenar, V.; Bax, A. *J. Am. Chem. Soc.* **1987**, *109*, 2221–2222.
(147) Patel, D. J.; Canuel, L. L. *Proc. Natl. Acad. Sci.* **1976**, *73*, 3343–3347.
(148) Reinhardt, C. G.; Krugh, T. R. *Biochemistry* **1977**, *16*, 2890–2895.
(149) Scott, E. V.; Jones, R. L.; Banville, D. L.; Zon, G.; Marzilli, L. G.; Wilson, W. D. *Biochemistry* **1988**, *27*, 915–923.
(150) Sobell, H. M.; Jain, S. C. *J. Mol. Biol.* **1972**, *68*, 21–34.
(151) Gorenstein, D. G.; Lai, K.; Shah, D. O. *Biochemistry* **1984**, *23*, 6717–6723.
(152) Shieh, H. S.; Berman, H. M.; Dabrow, M.; Neidle, S. *Nucleic Acids Res.* **1980**, *8*, 85–97.
(153) Goldfield, E. M.; Luxon, B. A.; Bowie, V.; Gorenstein, D. G. *Biochemistry* **1983**, *22*, 3336.
(154) Patel, D. J. *Acc. Chem. Res.* **1979**, *12*, 118–125.
(155) Wilson, W. D.; Jones, R. L. *Nucleic Acids Res.* **1982**, *10*, 1399–1410.
(156) Wilson, W. D.; Keel, R. A.; Mariam, Y. H. *J. Am. Chem. Soc.* **1981**, *103*, 6267–6269.
(157) Lai, K.; Gorenstein, D. G. *Biochemistry* **1989**, *28*, 2804–2812.
(158) Schroeder, S. A.; Roongta, V.; Fu, J. M.; Jones, C. R.; Gorenstein, D. G. *Biochemistry* **1989**, *28*, 8292–8303.
(159) Ott, J.; Eckstein, F. *Biochemistry* **1985**, *24*, 2530–2535.
(160) Fratini, A. V.; Kopka, M. L.; Drew, H. R.; Dickerson, R. E. *J. Biol. Chem.* **1982**, *257*, 14686–14707.
(161) Calladine, C. R. *J. Mol. Biol.* **1982**, *161*, 343–352.
(162) Sarai, A.; Mazur, J.; Nussinov, R.; Jernigan, R. L. *Biochemistry* **1988**, *27*, 8498–8502.
(163) Baleja, J. D.; Pon, R. T.; Sykes, B. D. *Biochemistry* **1990**, *29*, 4828–4839.
(164) Nilges, M.; Clore, G. M.; Gronenborn, A. M.; Piel, N.; McLaughlin, L. W. *Biochemistry* **1987**, *26*, 3734–3744.
(165) Powers, R.; Olsen, R. K.; Gorenstein, D. G. *J. Biomol. Struct. Dyn.* **1989**, *7*, 515–556.
(166) Lefevre, J. F.; Lane, A. N.; Jardetzky, O. *Biochemistry* **1987**, *26*, 5076–5090.
(167) Heinemann, U.; Alings, C. *J. Mol. Biol.* **1989**, *210*, 369–381.
(168) Nikonowicz, E. P.; Meadows, R. P.; Gorenstein, D. G. *Biochemistry* **1990**, *29*, 4193–4204.
(169) Pardi, A.; Hare, D. R.; Wang, C. *Proc. Natl. Acad. Sci. U.S.A.* **1988**, *85*, 8785–8789.
(170) Kaluarachchi, K.; Meadows, R. P.; Gorenstein, D. G. *Biochemistry* **1991**, *30*, 8785–8797.
(171) Ott, J.; Eckstein, F. *Biochemistry* **1985**, *24*, 253.
(172) Connolly, B. A.; Eckstein, F. *Biochemistry* **1984**, *23*, 5523–5527.
(173) Ott, J.; Eckstein, F. *Nucleic Acids Res.* **1985**, *13*, 6317–6330.
(174) Deslongchamps, P.; Atlani, P.; Frehel, D.; Malaval, A.; Moreau, C. *Can. J. Chem.* **1974**, *52*, 3651.
(175) Kollman, P.; Keepers, J. W.; Weiner, P. *Biopolymers* **1982**, *21*, 2345.
(176) Post, C. B.; Meadows, R. P.; Gorenstein, D. G. *J. Am. Chem. Soc.* **1990**, *112*, 6796–6803.
(177) Nikonowicz, E. P.; Meadows, R.; Post, C.; Jones, C.; Gorenstein, D. G. *Bull. Magn. Reson.* **1989**, *11*, 226–229.
(178) Gorenstein, D. G. *Organophosphorus Chemistry*; Marcel Dekker, Inc.: New York, 1993.
(179) Boelens, R.; Koning, T. M. G.; Kaptein, R. *J. Mol. Struct.* **1988**, *173*, 299–311.
(180) Boelens, R.; Koning, T. M. G.; van der Marel, G. A.; van Boom, J. H.; Kaptein, R. *J. Magn. Reson.* **1989**, *82*, 290–308.
(181) Borgias, B. A.; James, T. L. *J. Magn. Reson.* **1990**, *87*, 475–487.
(182) Benevides, J. M.; Wang, A. H. J.; van der Marel, G. A.; van Boom, J. H.; Thomas, G. J., Jr. *Biochemistry* **1988**, *27*, 931–938.
(183) Yanagi, K.; Prive, G. G.; Dickerson, R. E. *J. Mol. Biol.* **1991**, *217*, 201–214.
(184) Nikonowicz, E. P.; Roongta, V.; Jones, C. R.; Gorenstein, D. G. *Biochemistry* **1989**, *28*, 8714–8725.
(185) Patel, D. J.; Kozlowski, S. A.; Ikuta, S.; Itakura, K. *Biochemistry* **1984**, *23*, 3207–3217.

(186) Patel, D. J.; Kozlowski, S. A.; Ikuta, S.; Itakura, K. *Biochemistry* **1984**, *23*, 3218–3226.
(187) Kalnik, M. W.; Norman, D. G.; Zagorski, M. G.; Swann, P. F.; Patel, D. J. *Biochemistry* **1989**, *28*, 294–303.
(188) Hare, D.; Shapiro, L.; Patel, D. J. *Biochemistry* **1986**, *25*, 7456–7464.
(189) Chen, F. M. *Biochemistry* **1990**, *29*, 7684–7690.
(190) Chou, S. H.; Cheng, J. W.; Fedoroff, O. Y.; Chuprina, V. P.; Reid, B. R. *J. Am. Chem. Soc.* **1992**, *114*, 3114–3115.
(191) Lane, A.; Martin, S. R.; Ebel, S.; Brown, T. *Biochemistry* **1992**, *31*, 12087–12095.
(192) Kaluarachchi, K.; Gorenstein, D. G. Manuscript in preparation, 1994.
(193) Grzeskowiak, K.; Yanagi, K.; Prive, G. G.; Dickerson, R. E. *J. Biol. Chem.* **1991**, *266*, 8861–8883.
(194) Mauffret, O.; Hartmann, B.; Convert, O.; Lavery, R.; Fermandjian, S. *J. Mol. Biol.* **1992**, *227*, 852–875.
(195) Withka, J. M.; Swaminathan, S.; Beveridge, D. L.; Bolton, P. H. *J. Am. Chem. Soc.* **1991**, *113*, 5041–5049.
(196) Brahms, S.; Fritsch, V.; Brahms, J. G.; Westhof, E. *J. Mol. Biol.* **1993**.
(197) Baleja, J. D.; Germann, M. W.; van de Sande, J. H.; Sykes, B. D. *J. Mol. Biol.* **1990**, *215*, 411–428.
(198) Karslake, C.; Schroeder, S.; Wang, P. L.; Gorenstein, D. G. *Biochemistry* **1990**, *29*, 6578–6584.
(199) Karslake, C.; Botuyan, M. V.; Gorenstein, D. G. *Biochemistry* **1992**, *31*, 1849–1858.
(200) Gilbert, W.; Gralla, J.; Major, J.; Maxam, A. *Protein-Ligand Interactions*; de Gruyter: Berlin, 1975; pp 270–288.
(201) Lehming, N.; Sartorius, J.; Oehler, S.; von Wilcken-Bergmann, B.; Müller-Hill, B. *Proc. Natl. Acad. Sci.* **1988**, *85*, 7947–7951.
(202) Lehming, N.; Sartorius, J.; Kisters-Woike, B.; von Wilcken-Bergmann, B.; Müller-Hill, B. *EMBO J.* **1990**, *9*, 615–621.
(203) Caruthers, M. H. *Acc. Chem. Res.* **1980**, *13*, 155–160.
(204) Ptashne, M. *A Genetic Switch*; Cell Press: Cambridge, MA, 1986.
(205) Wharton, R. P.; Ptashne, M. *Nature* **1985**, *316*, 601–605.
(206) Wharton, R. P.; Ptashne, M. *Nature* **1987**, *326*, 888.
(207) Betz, J. L. *Gene* **1986**, *42*, 283–292.
(208) Betz, J. L. *J. Mol. Biol.* **1987**, *195*, 495–504.
(209) Ebright, R. H. *Protein Structure Folding and Design*; Oxender, D., Ed.; Alan R. Liss: New York, 1986; pp 207–219.
(210) Eisenbeis, S. J.; Nasoff, M. S.; Noble, S. A.; Bracco, L. P.; Dodds, D. R.; Caruthers, M. H. *Proc. Natl. Acad. Sci.* **1985**, *82*, 1084–1088.
(211) Koudelka, G. B.; Harrison, S. C.; Ptashne, M. *Nature* **1987**, *326*, 886.
(212) Lehming, N.; Sartorius, J.; Niemöller, M.; Genenger, G.; von Wilcken-Bergmann, B.; Muller-Hill, B. *EMBO J.* **1987**, *6*, 3145–3153.
(213) Adler, K.; Beyreuther, K.; Fanning, E.; Geisler, N.; Gronenborn, B.; Klemm, A.; Müller-Hill, B.; Pfahl, M. *Nature (London)* **1972**, *72*, 322–327.
(214) Wade-Jardetzky, N.; Bray, R. P.; Conover, W. W.; Jardetzky, O.; Geisler, N.; Weber, K. *J. Mol. Biol.* **1979**, *128*, 259–264.
(215) Buck, F.; Rüterjans, H.; Beyreuther, K. *FEBS Lett.* **1978**, *96*, 335–338.
(216) Wemmer, D.; Kallenbach, N. R. *Biochemistry* **1983**, *22*, 1901–1906.
(217) Zuiderweg, F.; Scheek, R.; Boelens, R.; van Gunsteren, R.; Kaptein, R. *Biochemie* **1985**, *67*, 707–715.
(218) Simons, A.; Tils, D.; von Wilcken-Bergmann, B.; Muller-Hill, B. *Proc. Natl. Acad. Sci. U.S.A.* **1984**, *81*, 1624–1628.
(219) Sadler, J. R.; Sasmor, H.; Betz, J. L. *Proc. Natl. Acad. Sci. U.S.A.* **1983**, *80*, 6785–6789.
(220) Betz, J.; Sasmor, H.; Buck, F.; Insley, M.; Caruthers, M. *Gene* **1986**, *50*, 123–132.
(221) Botuyan, M. V.; Keire, D. A.; Kroen, C.; Gorenstein, D. G. *Biochemistry* **1993**, *32*, 6863–6874.
(222) Karslake, C.; Wisniowski, P.; Spangler, B. D.; Moulin, A. C.; Wang, P. L.; Gorenstein, D. G. *J. Am. Chem. Soc.* **1991**, *113*, 4003–4005.
(223) de Vlieg, J.; Berendsen, H. J. C.; van Gunsteren, W. F. *Proteins: Struct. Funct. Genet.* **1989**, *6*, 104–127.
(224) Boelens, R.; Scheek, R. M.; van Boom, J. H.; Kaptein, R. *J. Mol. Biol.* **1987**, *193*, 213–234.
(225) Donlan, M. E.; Lu, P. *Nucleic Acids Res.* **1992**, *20*, 525–532.
(226) Cheung, S.; Arndt, K.; Lu, P. *Proc. Natl. Acad. Sci. U.S.A.* **1984**, *81*, 3665–3669.
(227) Patel, D. J.; Shapiro, L.; Hare, D. *Q. Rev. Biophys.* **1987**, *20*, 35–112.
(228) Barber, A. M.; Zhurkin, V. B. *J. Biomol. Struct. Dyn.* **1990**, *8*, 213–232.
(229) Page, M. I.; Jencks, W. P. *Proc. Natl. Acad. Sci. U.S.A.* **1971**, *68*, 1678–1683.
(230) Pearlman, D. A.; Kollman, P. A. *J. Mol. Biol.* **1991**, *220*, 457–479.
(231) Brown, I. D.; Shannon, R. D. *Acta Crystallogr. Sect. A: Cryst. Phys. Diffr. Theor. Gen. Crystallogr.* **1973**, *29*, 226.
(232) Jurnak, F. A.; McPherson, A. *Biological Macromolecules and Assemblies*; John Wiley and Sons: New York, 1984; pp 471–494.
(233) Pjura, P. E.; Grezeskowiak, K.; Dickerson, R. E. *J. Mol. Biol.* **1987**, *197*, 257–271.
(234) Hunter, W. N.; Brown, T.; Kneale, G.; Anand, N. N.; Rabinovich, D.; Kennard, O. *J. Biol. Chem.* **1987**, *262*, 9962–9970.
(235) Delepierre, M.; Van Heijenoort, C.; Igolen, J.; Pothier, J.; Le Bret, M.; Roques, B. P. *J. Biomol. Struct. Dyn.* **1989**, *7*, 557–589.